THE INFLUENCE OF FREE-STREAM TURBULENCE ON SEPARATION OF TURBULENT BOUNDARY LAYERS IN INCOMPRESSIBLE, TWO-DIMENSIONAL FLOW

J. Leith Potter
R. Joel Barnett
Carl E. Fisher
Costas E. Koukousakis

Final Report
NASA Research Grant NAG-1-483

22 December 1986

VANDERBILT UNIVERSITY
School of Engineering
Department of Mechanical & Materials Engineering
Nashville TN 37235

THE INFLUENCE OF FREE-STREAM TURBULENCE ON SEPARATION OF TURBULENT BOUNDARY LAYERS IN INCOMPRESSIBLE, TWO-DIMENSIONAL FLOW

J. Leith Potter
R. Joel Barnett
Carl E. Fisher
Costas E. Koukousakis

Vanderbilt University
Nashville, TN 37235
22 December 1986

Final Technical Report Prepared for
Langley Research Center
Under NASA Research Grant NAG-1-483

ABSTRACT

Experiments were conducted to determine if free-stream turbulence scale affects separation of turbulent boundary layers. In consideration of possible interrelation between scale and intensity of turbulence, the latter characteristic also was varied and its role was evaluated. Flow over a 2-dimensional airfoil in a subsonic wind tunnel was studied with the aid of hot-wire anemometry, liquid-film flow visualization, a Preston tube, and static pressure measurements. Profiles of velocity, relative turbulence intensity, and integral scale in the boundary layer were measured. Detachment boundary was determined for various angles of attack and free-stream turbulence.

The free-stream turbulence intensity and scale were found to spread into the entire turbulent boundary layer, but the effect decreased as the airfoil surface was approached. When the changes in stream turbulence were such that the boundary layer velocity profiles were unchanged, detachment location was not significantly affected by the variations of intensity and scale. Pressure distribution remained the key factor in determining detachment location.

TABLE OF CONTENTS

LIST OF SYMBOLS

C_f	Skin friction coefficient
C_p	Pressure coefficient, $(p-p_\infty)/(\rho_\infty U_\infty^2/2)$
H	Boundary layer shape factor
I_x	Integral scale of turbulence in streamwise direction
L	Unit of length
L_x	Dissipation length scale parameter
M	Grid mesh dimension
p	Pressure
Re	Reynolds number
R_u	Autocorrelation coefficient
T'	Relative turbulence intensity
S_t	Stanton number
t	Time
U	Streamwise mean velocity
u	Streamwise instantaneous velocity fluctuation
u'	Root mean square of u
X	Streamwise distance from grid to measurement station
x	Streamwise coordinate
y	Coordinate direction normal to and away from surface
z	Spanwise coordinate
α	Angle of attack
δ	Total boundary layer thickness
ρ	Density
Θ	Boundary layer momentum thickness

Subscripts

d	At detachment
e	Outer edge of boundary layer
o	Minimum stream turbulence (no grid)
t	At transition
x	Based on wetted streamwise distance
∞	Free-stream
.995	Refers to δ as defined where $U/U_e = 0.995$
1	At entrance to tunnel contraction section
2	At exit of tunnel contraction section
θ	Based on momentum thickness

LIST OF TABLES

LIST OF FIGURES

INTRODUCTION

This investigation was undertaken to learn if the scale of turbulence in the free stream has any influence upon the location at which boundary layer separation occurs in an adverse pressure gradient. Both free-stream turbulence intensity and scale recently have been reported to influence local skin friction coefficient (refs. 1-7). Thus, in view of the linkage of that factor with separation location provided by Townsend's analysis (ref. 8), it is implied that both free-stream turbulence intensity and scale may affect separation. If so, there would be concern about the varying turbulence scales in wind tunnels, air-breathing propulsion units, and numerous other internal flows. In addition, the possibility of optimizing flow-manipulating devices such as vortex generators would seem feasible. Flow separation and related aerodynamic phenomena are of great importance in many fields of fluids engineering.

In view of the prevalence of turbulent boundary layers in current practical situations, and also in consideration of the expected need to investigate turbulence intensities that would be rather high in the context of wind tunnel flows, this investigation has been focused largely on turbulent boundary

layers. Although laminar separation can occur at low Reynolds numbers, in circumstances of practical interest it will frequently be followed by transition of the unstable separated shear layer and subsequent reattachment as a turbulent boundary layer. The latter may separate still further downstream if it is exposed to a sufficiently strong positive pressure gradient. Thus, it is possible to have both laminar and turbulent separations within rather short streamwise distances.

This investigation was confined to subsonic, essentially two-dimensional flows. The evidence for a free-stream turbulence scale effect on skin friction seemed somewhat inconsistent (cf. refs. 3 and 4) at the time this work was planned, and it was thought that the simplest conditions of practical relevance should be chosen for study. The approach was, first, to determine if free-stream intensity and scale variations affect detachment and then to define the parameters that controlled the separation process. A subsonic wind tunnel with its associated pressure transducer and hot-wire anemometry systems and a 2-dimensional airfoil comprised the principal experimental tools used in this investigation.

It has been necessary to conduct an extensive experimental program to measure free-stream turbulence characteristics prior to investigating the influence of those parameters on separation. This report includes a summary of those data, which have been more fully covered in refs. 9 and 10. Also in connection with this research, there was an opportunity to acquire data on

laminar separation bubbles, i.e., laminar boundary layer separation followed by transition and reattachment. References 11 and 12 stemmed from that work.

The Separation Zone

Following Simpson (ref. 13) and others, separation is here taken to mean the entire process of breakaway and breakdown of a boundary layer from its bounding surface. The mean separated flow may be two- or three-dimensional. Although vanishing wall shear stress and flow reversal are usually associated with separation, these are only typical of two-dimensional separation with steady free-stream flow, and it is incorrect to assume that they are characteristic of three-dimensional separations or unsteady free streams.

It is essential to note that separation, like boundary layer transition, occupies a spatial zone. This can have important implications in connection with the interpretation of patterns in liquid surface films or boundary layer profiles measured with probes in a separation zone. "Separation" usually is presented without qualification as a single-point measurement. The following sketch indicates the nature of two-dimensional separation with steady free-stream flow, which is the category discussed in this report.

The Separation Zone

(Reference 13)

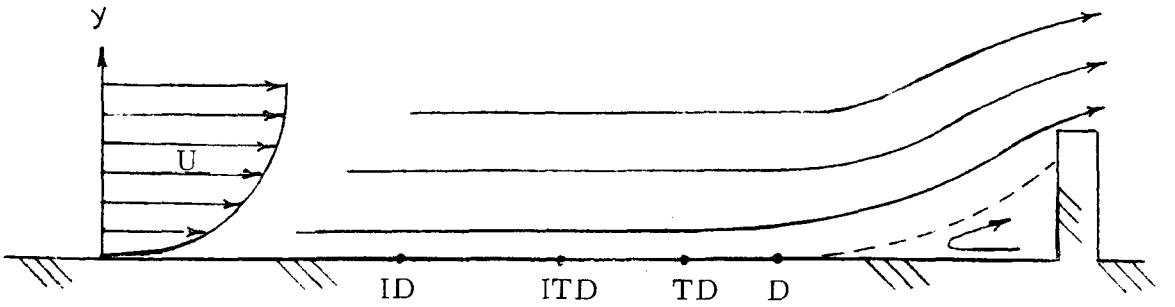

ID = incipient detachment (1% instantaneous backflow)

ITD = intermittent transitory detachment (20% instantaneous backflow)

TD = transitory detachment (50% instantaneous backflow)

D = detachment (mean shear stress = 0)

One would expect that lengths between the defined points may vary with the conditions in a given case. However, there does not seem to be much information on this particular aspect of the problem.

The lack of data from probing within separated flow regions is repeatedly remarked in survey papers, c.f. ref. 13. High turbulence and reversals in mean flow direction, which are

characteristic of the separation zone, make the hot-wire anemometer unreliable despite its rapid response. Pitot tubes also suffer in such environments, and the lag in response of their transducers is an added problem. Double-headed pitot probes have been used in separation zones to gain directional capability, but their other problems, including obstruction of the flow, remain. Much can be learned from flow visualization techniques, but extremely complex flow fields often are generated in separation zones, and the interpretation of surface liquid film or "paint" patterns and other visual evidence is not always certain.

Turbulence Intensity

Free-stream relative turbulence intensity throughout this discussion is taken to be

$$T'_\infty = \sqrt{\overline{u^2}}/U_\infty = u'/U_\infty \qquad (1)$$

where

$\overline{u^2}$ = mean square of the fluctuating component of the mean free-stream velocity, U_∞

A cartesian coordinate system with x in the streamwise direction and y normal to both x and the wall is adopted. Orthogonal to these is a z-axis considered to lie in the spanwise direction. As discussed in ref. 14, a hot wire normal to the x-axis is exposed to fluctuating velocity components along all three axes, but under the conditions prevailing in an experiment such as the present one, the wire output is dominated by the velocity along

the x-axis.

Turbulence relative intensity within the boundary layer is defined as

$$T' = u'/U \qquad (2)$$

where

U = mean streamwise velocity at height y within boundary layer

Turbulence Scales

To describe turbulent motion quantitatively, in addition to relative intensity, the concept of turbulence scales has been formulated, (cf. refs. 15-16). Scales in time and in space, as well as scales in longitudinal and transverse directions, are considered.

Defining the scales of turbulence usually involves correlations between velocity components separated in either time or space. In either case, the correlation will be a function of time lapse or distance between the points. Distinctions are made between small fluid elements (fluid "particles") and larger elements (fluid "lumps"). The former are comparable to the micro scales, the latter comparable to the integral scales. Eulerian and Lagrangian descriptions are useful. In the first, the variation of a property with respect to a fixed coordinate system is considered; in the latter, the variation of the property connected with a given fluid particle or fluid lump is determined.

Traditionally, the integral scale usually has been used in efforts to determine the role of turbulence scale in connection with drag, heat transfer, separation, transition, etc. However, other scales in the spectrum of turbulence have been identified, and several recent reports of studies of the influence of free-stream turbulence on boundary layers present discussions based exclusively on a dissipation length scale parameter (e.g. refs. 5-7). The latter is attractive in that it is generally easier to measure.

With regard to the scale of most influence on boundary layer separation, the issue would appear to be whether gradient-type transport of turbulence properties, related to the micro- or dissipation lengths, or transport by bulk movement related to the integral scales is the dominant process. One is attracted to the idea that bulk movement, and therefore integral scale, is the most likely candidate. The almost universal choice of early investigators of scale effect on boundary layers has been the integral scales (e.g., ref. 17). Numerous other examples of this choice could be cited. However, in 1974, Bradshaw (ref. 18) proposed that a dissipation length scale parameter be used for interpretation of the effects of turbulence scale upon boundary layers, and this is the path followed by several of the recent investigators. According to ref. 18, the longitudinal dissipation length scale is proportional to and of the order of the integral scale. Both scales were measured in the present case, and each is defined here.

Integral Scale:

References 15-16, for example, contain detailed discussions of this topic, so only the particular approach followed in the present work is described. If the fluctuating velocity component u is measured at times t and (t + r), a correlation coefficient may be defined as

$$R_u = \overline{u(t) \cdot u(t + r)}/[\overline{u^2}(t) \cdot \overline{u^2}(t + r)]^{0.5} \qquad (3)$$

When R_u is determined for a range of time delays, a curve such as shown in Fig. 1 is produced. A quantity defined as

$$t = \int_o^\infty R_u \, dt \qquad (4)$$

is multiplied by the mean velocity, U, to give a length I_x which represents the typical x dimension of the energy-containing eddies in the flow. This is the integral scale used hereafter in this report. Considerations of other coordinate directions and velocity components leads to the other integral scales. In practice the integration in Eq. (4) is terminated where R_u first becomes zero.

Dissipation Length Scale Parameters:

A streamwise dissipation length scale parameter is defined following refs. 15 and 18, viz.,

$$Lx = -(\overline{u^2})^{1.5}/[U_\infty(d\overline{u^2}/dx)] \qquad (5)$$

The longitudinal turbulence energy produced by grids typically decays according to a relation such as

$$(\overline{u^2}/U_\infty^2)^{-n} = C(X-X_o)/M \qquad (6)$$

where $\overline{u^2}$ = mean u^2 value

C = a constant

M = grid mesh size

X = distance downstream from grid and

X_o = a constant

There is frequent need for an effective starting length to be used in order to fit Eq. (6) to experimental data, thus X_o is present to accommodate that need. When Eq. (6) is differentiated and combined with Eq. (5), it is found that

$$L_x/M = nC^{-0.5/n}[(X-X_o)/M]^{1-0.5/n} \tag{7}$$

It is interesting to note that this parameter will increase with X/M if $n > 0.5$ but decrease if $n < 0.5$. One supposes that the value of n is affected if turbulence originates downstream of the grid. For example, turbulence may be generated in a diffuser or at a wind tunnel fan and propagate upstream in subsonic flow. When that happens, the rate of turbulence decay is altered. The possibility of turbulence "feed-in" downstream of a grid cannot be ignored for many subsonic wind tunnels.

The boundary layer on an airfoil in a wind tunnel was studied in this research. Therefore, free-stream turbulence characteristics were measured at a point on the tunnel centerline immediately upstream of the station where the airfoil leading edge was later located. A catalog of T'_∞, $I_{x\infty}$, and $L_{x\infty}$ values was compiled for five turbulence-producing grids located at various distances upstream of the test section. Examples of these data are shown later.

The previous investigations of the combined effect of both

T′ and I_x or L_x on local skin friction or Stanton number (cf. refs. 1-7) led to the several empirically determined correlation parameters listed below. These parameters collapsed $\Delta C_f/C_{fo}$ or $\Delta S_t/S_{to}$ data to single curves with moderate scatter, within the scope or range of conditions covered in the referenced studies:

$100\ (u'/U_e)/[(L_x/\delta) + 2]$ . . . ref. 5

$100\ (u'/U_e)/[(L_x/\delta) + 2] \cdot [3\ \exp(-Re_\theta/400) + 1]$ . . . ref. 6

When Castro (ref. 7) extended the $\Delta C_f/C_{fo}$ measurements to lower Re_θ than previously covered he achieved the correlation of his and Hancocks′ (ref. 1) data by plotting

$$(\Delta C_f/C_{fo})\ \{\ 1 + 10/[F^2\ \exp(-Re_\theta/400)]\ \}$$

as a function of F, where

$$F = 100\ (u'/U_e)\ /\ [(0.5L_x/\delta) + 2.5]$$

In all cases δ is defined to correspond with $U/U_e = 0.995$.

Although the above parameters vary, they all suggest that the effects of T′ and I_x or L_x are opposite, i.e., C_f increases with T′ but decreases as I_x or L_x increase.

A few words are necessary regarding the relationship of I_x and L_x. In ref. 18 it is remarked that

$$L_x \approx 4.5\ I_x$$

while, in ref. 6, it is noted that

$$L_x \approx 1.5\ I_x.$$

In the experiments to be described, neither of the above relations holds. In the case of ref. 18, it seems that reference is made to grids installed upstream of the working section in a duct of constant area. In ref. 6, it is clear that the grids

were mounted upstream of a contraction in area preceding the test section. Both configurations were used in the present work.

Interaction of Free-Stream and Boundary Layer Turbulence

It is perhaps premature to present this topic, because it will have to be taken up again when results of this investigation are discussed. However, for background to the experimental data as they are presented, some of the physical concepts applicable to the present study should be mentioned. These are drawn principally from refs. 4, 7, 13, and 18.

Meier (ref. 4) comments that "Maximum values of the skin friction coefficient at T'_∞ = const. were obtained at length scales in the order of the boundary layer thickness." Simpson (ref. 13) observes that "the backflow region is strongly dominated by turbulent fluctuations that are greater than, or at least comparable to, the mean velocities . . . ." Further, he states that there is no location with backflow all of the time. This is significant in connection with efforts to measure velocity profiles in separation zones.

In the introductory part of ref. 18, Bradshaw suggests tentatively, based on various evidence, that "free-stream turbulence reduces the ability of the existing shear layer turbulence to transfer momentum or scalars, and/or that the shear-layer turbulence reduces the mixing ability of the free-stream turbulence that adjoins it." At another point, he asserts that "it appears that large-scale free-stream turbulence has no

direct effect on turbulence structure. . . ." Also, "If the intensity and length scale of the free-stream turbulence are of the same order as those of the shear layer - as they must be to produce significant effects. . . ." Lastly, "It is demanded by logic, and confirmed by experiment, that the effect of free-stream turbulence is first felt by the outer layer."

Castro (ref. 7) writes that, "It appears that the addition of free-stream turbulence significantly reduces the Reynolds number effects on u^2 and there is even a suggestion that at the highest value of FSTP (free-stream turbulence parameter) . . . the effect is reversed." The FSTP referred to is

$$(u'/U_e)/[(L_x/\delta) + 2]$$

This section has been included to provide background to the remainder of the report. The linkage between the earlier work, most of which reported the effect of free-stream turbulence on C_f or S_t, and separation is offered by Townsend's analysis (ref. 15). It is shown there that C_f is a factor affecting separation location. That relationship is made use of later when the present data are discussed.

EQUIPMENT and TECHNIQUES

Wind Tunnel

The Vanderbilt University Engineering School Wind Tunnel is shown in Figures 2 and 3. A top view of the tunnel is not shown because the structure is of square cross section upstream of the diffuser, and the latter component varies from square to circular as it extends downstream. Except for the fan section, the tunnel shell is made of fiberglass, giving a very smooth interior surface. A summary of flow conditions is presented in Table 1.

The smaller, higher speed, 0.4-m section is the normal test section, and all subsequent comments will pertain to that area unless specific reference is made to the 1-m section.

A shroud, honeycomb, and two screens are installed at the wind tunnel entrance. The honeycomb is fabricated of plastic impregnated paper having a thickness of 0.2 mm. There are two layers making up the honeycomb. In each layer the cells, or openings, are approximately triangular in cross section, with a base of 9.5 mm and height of 8 mm. Streamwise dimension of the assembly is 64 mm, giving a length-to-hydraulic diameter ratio of approximately 7.

Two fiberglass screens with 6.3 mesh/cm (16/in.) are installed to reduce turbulence. Additional screens may be inserted if it is desired to study phenomena requiring very low free-stream turbulence. Relative turbulence intensity in the

test section is approximately 0.16 percent with the present set of screens. Figure 4 is a plot of T_{u_∞} as a function of free-stream velocity.

Velocity distribution laterally across the 0.4-m test section, measured by hot-wire and pitot-static probes, is constant to within ± 1 percent in the central 0.3 m (12 in.) at a mean velocity of 60 m/s (200 fps). Longitudinal velocity gradient in the test section is virtually zero at all of the usual test conditions.

A flexible coupling at the downstream end of the diffuser reduces vibration that would be caused by the centrifugal fan and motor. The laboratory floor is of thick concrete and quite rigid. However, at higher speeds there is a small amount of vibration in the tunnel shell, so sensitive probes are mounted onto the laboratory floor or to heavy structural steel beams above the wind tunnel. Most of the flow surveys discussed later were made with hot-wire or pressure probes mounted to the overhead structure as shown in Fig. 5

Figure 6 shows the airfoil with the spoiler used in this investigation, and Fig. 7 shows the fiber-optic, surface-sensing device that enables the delicate hot-wire sensor to be positioned within a quarter of a millimeter or less distance from a solid surface without being broken by contact. The latter is a fiber-optic, light-emitting auxiliary probe (A) which is mounted on the same micrometer system that positions the flow probe (B). Light from a photo-flood light outside of the tunnel passes through a

fiber-optic filament and is emitted from the end of the tube (A), which is adjusted so that it is perpendicular to the model surface (C). When the end of this tubular probe contacts the model surface, the circular spot of light beamed from its open end (D) is extinguished. This provides a sufficiently precise and repeatable indication of hot-wire distance from the model surface when the end of tube (A) touches the surface and the displacement between hot-wire flow probe and light-emitting probe tip has been determined. The latter dimension is measured in the present case by a telescope equipped with a micrometer and movable cross hairs. In practice, the two coupled probes are displaced so that the very fragile hot wire sensor does not contact the model surface when the light probe touches that surface. The principal advantage of this technique for indexing probe position is that it is usable when the model surface is not electrically conducting and an electrical signal of surface-to-probe contact cannot be obtained.

Pressure and Hot-Wire/Hot-Film Systems

The Vanderbilt Wind Tunnel is equipped with a Scanivalve Corporation DSS 24C MK3 electronic switching-valve pressure transducer system. When this is used in conjunction with a manually-operated Norgren Fluidics 10-port switch, up to 34 pressure measurement channels are available. Because the Scanivalve pressure transducer range is too high for accurate results in the present program, a MKS Baratron Model 170M-6C

precision pressure transducer with a full-scale range of 100 mm Hg was used.

Three channels of hot-wire instrumentation are available. These include one Thermo Systems, Inc. (TSI) Model 1050 and two TSI Model 1010 anemometer systems. Each anemometer channel has a linearizer, a TSI Model 1052A being used with the 1050 anemometer and TSI Model 1072 linearizers with the 1010 anemometers. A TSI 1015C Correlator is available for correlation of signals from the anemometers. However, it was more convenient and accurate to utilize digital signal processing techniques made possible by availability of an analog-to-digital convertor and an Apple IIe computer connected to VAX and DEC mainframes.

The hot-wire voltage measurements, D.C., rms, and mean square, were obtained with a TSI Model 1076 digital voltmeter. This instrument may be operated with time constants of 0.1, 1.0, 10 and 100 seconds.

Data acquisition was accomplished with an Interactive Structures, Inc., Model AI13 analog-to-digital converter coupled to an Apple IIe computer. Experiments were conducted to determine the effects of sampling time and frequency, and the optimum schedule was selected. Computer programs written to process the hot-wire data and compute turbulence properties are in Appendix I of this report.

The hot-wire/hot-film probes were of convention design. The hot-wire sensors were platinum coated tungsten on gold plated needle-type supports. Diameter of sensing element is 3.8 μ

(0.00015 in.) and the length is 1.27 mm (0.050 in.). Corresponding dimensions of the hot-film probe sensors were 51 μ (0.002 in.) and 1.0 mm (0.040 in.). The sensor films were platinum with an alumina coating. Fused quartz substrates and gold plated needle-type supports were used. A photograph of a hot-wire probe may be seen in Fig. 7.

Although some early measurements were made with hot-film probes, it was discovered that those gave erroneous (high) u′ at free-stream speeds above roughly 40-45 m/s (140 fps). This problem was not studied in detail, once the trouble was isolated to the probe type. However, it is apparent that the much greater diameter of the hot-film sensor led to much lower frequencies of vortex shedding (cf. ref. 19), and it seems likely that this may have affected the readings. Probe vibration was also suspected, but the addition of stiffening fillets to the sensor-supporting needles did not eliminate the trouble. It is noteworthy that a similar failing was found later when using a "boundary-layer" type of probe with long, curved, needle-like supports for the sensor, even though these had a hot-wire sensor. In that case, it seems most probable that the long support needles must have vibrated. Changing to stiffer type of probe seen in Fig. 7 apparently avoided the problem. All hot-wire data presented in this report were obtained with probe configurations that performed best and seemed free of spurious influences after a period of trial testing. Experiments were performed to confirm that the support strut of the probe shown in Fig. 7 did not

affect the sensor signal.

It was necessary to make a small correction to the hot-wire voltages when the wire was very close (< 1 mm) to the airfoil surface. Heat transfer to the cooler airfoil caused hot-wire voltages to falsely indicate higher velocities. An example of this effect is shown in Fig. 8. The correction procedure followed ref. 20.

Another type of error becomes important when turbulence intensity levels are above the order of 10%. Near the airfoil surface in the separation zone, turbulence intensities of 10 to 50% were recorded. Following Bradshaw (ref. 14) a maximum error in T' of approximately +11% is estimated for the most adverse conditions for which data are given in this report. Inasmuch as that one case is only used as a qualitative example of high T' encountered in the separation zone, and all other corrections would be within the uncertainty band of the data, no corrections for high-turbulence error were made.

Skin friction measurements were made with the Preston tube shown in Fig. 9. Outside diameter at the entrance was 7.1 mm (0.028 in.). The pressure was read with the MKS Baratron system. The procedure followed ref. 21, and it was found that the parameters in the present case fell within the range covered in that reference. Effects of pressure gradient on Preston tube data were evaluated following ref. 22 and found to be negligible for the measurements reported here.

Detection of Detachment By Liquid Films

Liquid films of various solutions were painted onto an airfoil and tested in the tunnel. It was found that a mixture of the following approximate proportions (by volume) served our purpose:

50 percent water	[Optimum proportions
35 percent dry powdered poster paint	varied with tunnel
10 percent glycerine	speed. This was
5 percent Kodak Photo Flo.	typical.]

This solution was brushed onto an airfoil surface that had been wetted with a film of soapy water. Air flow was immediately started, and the drying liquid film was observed until an unchanging indication of "detachment" was seen.

Photography of the dried paint had to be done with the aid of a pair of plane mirrors because of the confined area and difficulty of access created by other apparatus. However, this technique was quite successful and only involved the extra work of installing and removing the mirrors between wind tunnel runs.

Photographs and tabulated data are presented later where the interpretation of the paint results is addressed. In general, very satisfactory information was obtained, both regarding separation and the quality of two-dimensionality of the flow over the airfoil. The streamwise streak lines visible in the dried paint are seen to be parallel to the free stream and normal to the spoiler on the airfoil.

The Airfoil

An airfoil was chosen to be the body on which to study separation because it is obvious that one of the principal areas of application of this research is that of airfoil and wing design. Figure 10 is a sketch of the airfoil. When installed, it nearly spanned the test section of the wind tunnel. End plates of relatively large size were fitted initially, but the end-plate area above the airfoil surface was soon cut away to avoid boundary layer development in the corners between the airfoil upper or working surface and the plate. Leaving end plates extending well beyond the lower surface seemed sufficient to prevent excessive air spillage into the region of the boundary layer surveys on the upper surface, and flow-visualization by the liquid-film or paint technique revealed a larger span of two-dimensional flow without the interference of the boundary layer on the upper area of the end plate.

Orifices for pressure measurement were located at the nominal stagnation point and every 1.27 cm (0.50 in.) downstream on the upper surface. Angle of attack could be varied, but most experiments were conducted with an angle of 1 deg. It was found that better, i.e., two-dimensional upper surface flow existed if a relatively low angle of attack was maintained and separation was caused by a spoiler, as shown in Fig. 10. This also imposed less aerodynamic load on the airfoil and mountings, so that there was less movement under load and more precise probe positioning was possible.

Grids and Effects of Wind Tunnel Contraction Section

Five different grids were used in the course of this investigation. Figure 11 gives the dimensions. It will be noted that Grids 1-3 were mounted in the tunnel upstream of the contraction that separates the 1-m and the 0.4-m test sections. Grids 4 and 5 were mounted at the downstream end of that contraction, i.e., at the upstream end of the 0.4-m test section.

Streamwise positions of Grids 1-3 were variable. Continuous tracks and movable mounting clips made that possible. However, Grids 4 and 5 were located at only one streamwise station as already specified. Figure 12 shows some of the grids.

It is shown in refs. 9, 10, and 23 that the effect of a contraction in cross section area upon stream turbulence is dependent on the character of the turbulence entering the contraction. Passage through a contraction between grid and hot-wire probe stations also alters the relationship between I_x and L_x. In the present case, the wind tunnel contraction area ratio is 6.2 (geometric) or 6.67 (based on measured center line velocities). Integral scales were measured at the entrance and at the exit of the contraction section, in a brief investigation of this phenomenon, and it was found that a magnification of integral scale occurred at all velocities and turbulence intensities. Figure 13 presents the measurements of I_{x2}/I_{x1} as a function of T_1'. I_{x1} does not appear to be a factor within the range of these data. Two empirical relationships roughly fitting the data for $1.5 < T_1'\% < 6$ are

$$I_{x2}/I_{x1} \simeq 1.31 + 2.67/T_1'\% \quad (8)$$

or $$I_{x2}/I_{x1} \simeq 3.71/(T_1'\%)^{0.46} \quad (9)$$

Figure 13 also shows these equations but it has to be emphasized that they are only based on these limited observations.

It may be significant that the contraction section where these data were obtained has a streamwise length that is 0.775 times the lateral dimension of its entrance and is of square cross section. The change in turbulence intensity as flow passes through an area contraction has been found to be largely dependent on the area or velocity ratio alone (cf. ref. 24), although more complex relationships have been published (ref. 25). However, the possibility of the rate of change of velocity being a factor in determining the ratio of I_{x2}/I_{x1} should not be overlooked.

Turbulence intensity ratios (T_2'/T_1') corresponding to the data in Fig. 13 average 1/6, which is very nearly identical to the wind tunnel contraction ratio, A_2/A_1. Figure 14 demonstrates that this result is consistent with data for some NASA tunnels given in ref. 24. On this subject, it should be noted that some decline in T' would occur over a length of constant area duct, so that all of the decrease in T' shown in Fig. 14 cannot be credited to the contraction in area alone.

Table 2 lists the T_∞' and $I_{x\infty}$ values that made up the menu of free-stream turbulence conditions available for selection in the investigation of separation. Having a range of T_∞' with $I_{x\infty}$ approximately equal to turbulent boundary layer thickness on the

downstream one-half of the airfoil chord was a goal. The damping effect on T'_{∞} exerted by the contraction section made it difficult to obtain higher T'_{∞} using grids 1-3. Therefore, grids 4 and 5 were fabricated and installed downstream of the contraction. This produced higher levels of T'_{∞} but the position 30 grid mesh lengths upstream of the airfoil leading edge for grid 4 and 15 mesh lengths for grid 5 was viewed with some apprehension because of possible flow nonuniformity. This concern was abated when a survey across the stream in the test section showed very acceptable uniformity of turbulence intensity. These data are presented in Fig. 15. The separation data obtained when grids 4 and 5 were used appear to be consistent with the results obtained when grids 1, 2, and 3 were used.

EXPERIMENTAL RESULTS AND ANALYSIS

Pressure Distribution and Transition

Figure 10 shows the airfoil and spoiler arrangement. The pressure distribution on the airfoil for angles of attack of 1, 3, 5, and 9 deg and free-stream speed of 50.5 m/s are presented in Figs. 16 a-d.

The location of boundary layer transition with no trips was determined by moving a hot-wire probe longitudinally along the surface at y = 0.15 mm and recording T′. The results are given in Fig. 17 for two unit Reynolds numbers. With $Re_\infty/m = 3.15 \times 10^6$ the values of $Re_{\infty t}$ are 6.07×10^5 for the beginning of transition and roughly 9.6×10^5 at the end of transition. When $Re_\infty/m = 4.00 \times 10^6$, transition began at $Re_{\infty t} = 7.12 \times 10^5$ and was completed at $Re_\infty = 8.74 \times 10^5$. Because it was preferable to conduct most of the experiments with $U_\infty = 50.5$ m/s, which corresponds to $Re_\infty/m = 3.15 \times 10^6$, trips were used to assure a fully turbulent boundary layer at the beginning of the adverse or positive pressure gradient on the airfoil. Again, a hot-wire probe was used to verify the desired fully turbulent boundary layer while using a trip of minimum height.

Detachment Locations

Figures 18 and 19 are examples of the data on separation as determined by the liquid-film technique. The small scale shown on the right-hand side in all overhead photos is pushed against

the upstream face of the spoiler. Numerous repetitions of the liquid-film measurements demonstrated excellent consistency of results. Before proceeding to discuss these data it is necessary to more precisely relate these observations to the terms in the sketch of the separation zone given in the Introduction. These photographs and numerous other examples of the liquid-film all display the major features sketched below.

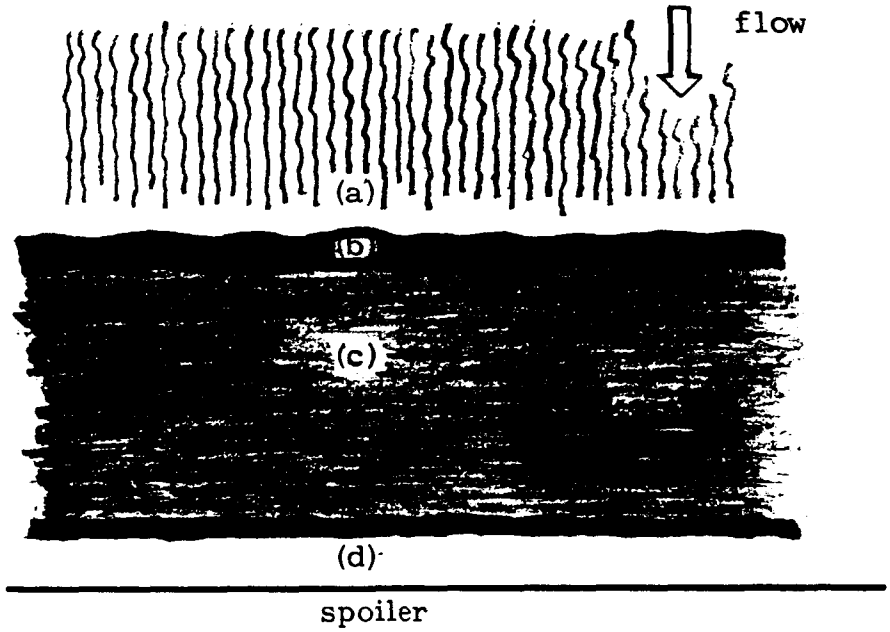

(a) = region approximately 1 cm in streamwise extent believed to be an area of intermittent backflow containing the ID and ITD boundaries defined earlier, following ref. 13. Paint in this area apparently is swept downstream where it contributes to formation of (b).

(b) = highly repeatable, narrow, heavy band of paint

believed to indicate near 50% instantaneous backflow, i.e., the TD station of ref. 13. Its prominence in the photos is partly due to its light-reflecting property. Detachment appears to occur essentially at the downstream edge of this band, making the TD and D stations very close together in this case.

(c) = an area several cm in streamwise extent where relatively low and random surface shear is evident. When the paint in this region was not overflowed by paint from other regions, it remained smooth and uniform while it dried.

(d) = highly repeatable, roughly 1-cm region at the foot of the spoiler where the surface is cleansed of paint by energetic vortical flow. The paint is swept upstream to the rear boundary of region (c).

Hot-wire and small impact-pressure probes were used to survey the regions (a-d), but the large magnitudes of fluctuating velocities and intermittency of velocity directions make probes of these types ineffective for determining details of flow near the surface in separation regions. (Use of a special laser-Doppler anemometer for this type of measurement is reported in ref. 26.) The typical, orderly velocity profiles with reversed flow near the solid surface that are often sketched when separation is discussed qualitatively do not adequately portray the intermittency and transitory patterns of real separation.

Further in regard to interpretation of the mean detachment

station, typical surface static pressure distributions across the separation zone are shown in Figs. 20 a-b. The "detachment" label in these figures is placed where the paint band (b) was located. It will be noted that the pressure coefficient did not reach a constant value at the designated detachment, but it did become constant a short distance downstream. This feature is common to many similar examples of pressure distributions with separation present. Thus, it seems justified to conclude that the dark paint band (b) in the photographs marks the upstream boundary of detached flow.

The Influence of T'_∞ and $I_{x\infty}$

Table 3 and Figs. 21 - 22 present detachment station, x_d, at corresponding T'_∞ and $I_{x\infty}$, as determined in this investigation of subsonic, turbulent boundary layers in typical adverse pressure gradients on the suction side of a two-dimensional airfoil. Angles of attack and free-stream velocities are indicated with the data in Table 3. Figures 21 and 22 correspond to α = 5 deg and 50.5 m/s. Tables 4 and 5 present data selected so that either T'_∞ or $I_{x\infty}/\delta$ was nearly constant while the other parameter varied. This format makes it easier to see how or if each turbulence parameter independently influenced detachment point. The airfoil was at α = 5 deg. and 50.5 m/s conditions when the data of Tables 4 and 5 were recorded.

The range of T'_∞ adequately represents wind tunnel flows and the higher turbulence of some other types of internal flows. As

planned, the free-stream integral scales are approximately equal to the boundary layer thicknesses upstream of the separation zone. It will be recalled that several previous investigators have concluded that this should lead to the maximum influence on surface shear stress. As Table 3 shows, the boundary layer thickness grew rather rapidly between the mid-chord and detachment stations. Thus, $I_{x\infty}$ generally fell between the values of $\delta_{.995}$ at x = 22.1 cm and x = 29.7 cm in these experiments. The ratio $I_{x\infty}/\delta_d$ given in the tables is based upon $\delta_{.995}$ at x = 29.7 cm, which is approximately the detachment station in all cases. If $\delta_{.995}$ at x = 22.1 cm were used, all ratios would be approximately doubled because the boundary layer thickness grew rapidly toward detachment.

The evidence in the tables and figures seems decisive; in the range of T'_∞ and $I_{x\infty}$ investigated, neither parameter had a significant effect on x_d. All measurements were repeatable to a very satisfactory degree, and no anomalies were observed. When confronted with this result, the decision was made to "back-track" and briefly check the influence of free-stream turbulence on skin friction.

Measurements of C_f

Earlier investigators (e.g., refs. 2 and 18) have reported on this, and it was seen as a way to determine if the present experiments were consistent with the related previous investigations. Failure in this test would point to some defect

in the present experiments. Therefore, a Preston tube was used to determine C_f at mid chord for several values of T'_∞ . Results are presented in Fig. 23.

Inspection of figures presented in refs. 6 and 7 reveals that the data on $C_f/C_{fo} = f(T'_\infty)$ typically scatter across the band drawn in Fig. 23. It has already been remarked in the previous section that there is agreement among refs. 3 - 7 that either integral length scale or dissipation length parameter also is a factor that should be incorporated into the correlation of C_f/C_{fo} with free-stream turbulence. However, the best form for this correlation parameter seems to be uncertain, and in any event, it apparently will be a weaker factor than T'_∞ . Therefore, Fig. 23 implies that the present experiments are consistent with earlier results, and no suspicious discrepancy is evident.

Comparisons With Prediction Methods

The final step in confirming the detachment results was the comparison of the measured x_d with predictions by Stratford's (ref. 27) method. That result is seen in Table 6. When making the calculations of x_d, the experimental C_p distributions were used.

The designations Strat. 1 and Strat. 2 refer, respectively, to the version of Stratford's method originally presented in ref. 27 and the modified method proposed by Cebeci, et al. in ref. 28. The modified version incorporates a small change in the critical

value of Stratford's separation criterion. In both cases, the initial length of laminar flow and favorable pressure gradient that existed on the airfoil in these experiments is taken into account. When the modification recommended by Cebeci, et al. is made, Table 6 shows excellent agreement between Strat. 2 and experiment.

Inasmuch as the surface shear stress or C_f appears directly in Townsend's method for predicting x_d (ref. 8), a brief examination of the effect of increased C_f caused by elevated free-stream turbulence was carried out. This was based on the faired curve for the "present data" in Fig. 23. That curve lies close to the Simonich and Bradshaw curve within the range of T'_∞ in Fig. 23.

The calculations by Townsend's method generally agreed closely with the results obtained by Stratford's method, as demonstrated in Table 7. However, in a number of cases Townsend's procedure failed to predict detachment, and Stratford's method gave better results. Use of the modified Townsend method proposed by Hahn, et al. (ref. 29) was even less successful in those cases. When either C_{fo} or C_f corresponding to elevated turbulence (from Fig. 23) were used in the Townsend procedure for predicting x_d, the difference was insignificant.

Once again, it should be remarked that the experimental pressure distributions were used for all of the x_d calculations. The Townsend method actually forecasts the C_p at detachment. When detachment occurs at a C_p lower than predicted, the

predicted value is not attained and there is simply no solution.

Interaction of Free-Stream and Boundary Layer Turbulence

In consideration of the basic data, the overall consistency of all results, and the generally very good agreement found where there were check points provided by related results from other investigators, the earlier statement that there is minimal influence of moderate levels of free-stream turbulence on x_d is now more strongly advanced. Of the pair of characteristics, T'_∞ and $I_{x\infty}$, neither the usually stronger parameter T'_∞ nor the weaker $I_{x\infty}$ were found to have a measurable linkage with x_d at the levels investigated. The fundamental factor would seem to be the weak penetration of free-stream turbulence into the inner part of the turbulent boundary layer. In pursuit of this subject, profiles of U/U_e, T' , and I_x were measured at the stations x = 22.1 cm and x = 29.7 cm for different levels of T'_∞ . The former station is well upstream of the separation zone, while the latter station is in the upstream or early part of that zone. The results for x = 22.1 cm are shown in Figs. 24 - 26.

It will first be noted that change of T'_∞ from 0.16% to 3.16% had no effect on thickness of the boundary layer. The effect of that increase in T'_∞ is apparent in Fig. 25, and the increase of $I_{x\infty}$ also affects the profiles in Fig. 26. Next, the profiles of the same quantities at x = 29.7 cm are examined to learn how these turbulence properties change as the separation zone is entered.

Figures 27 - 29 display the profiles of U/U_e, T' , and I_x found at x = 29.7 cm. At this station (approximately at detachment), the situation is different in some respects from the x = 22.1 cm case just discussed. First one notes that changing T'_∞ again has an insignificant effect on the velocity profile. However, boundary layer thickness has increased markedly in comparison to the data for x = 22.1 cm.

The response of the boundary layer profiles to free-stream turbulence intensity and scale shown in Figs. 28 and 29 is similar to that found for those two parameters at x = 22.1 cm. These figures again show that the feed-in of free-stream turbulence characteristics weakens as y decreases and has reduced influence near the solid boundary.

A significant point well illustrated in Figures 25, 28 and 30 is that T' near the solid surface in the separation zone is much greater than the free-stream turbulence intensity. That strongly implies that only very high levels of free-stream turbulence may have any possibility of affecting separation. Of course, very great turbulence will also affect boundary layer growth and thereby affect the pressure distribution. The latter factor is dominant in regard to detachment and could easily overshadow any direct effect of changes in turbulence intensity within the boundary layer.

Figures 26 and 29 show that integral scales within the boundary layer had a characteristic profile that contained scales lower than free-stream near the wall and greater than free-stream

in the outer part of the boundary layer. There was a consistent increase of I_x as $I_{x\infty}$ increased, but the effect was small at the y - values deep within the boundary layer.

When examining the profiles of I_x, some consideration should be given to the nature of the autocorrelation procedure and the degree of uncertainty. A repeatability of approximately ± 10% is indicated by $I_{x\infty}$ measured on different days under the less favorable signal - to - noise conditions corresponding to low free-stream turbulence. For a given run or profile in Figs. 26 and 29, the uncertainty must be less because T′ is much greater, making signal - to - noise ratio higher, measurements were taken within a brief time interval, and only one wind tunnel run was involved. However, conditions near the outer edge of turbulent boundary layers are such as to impose greater scatter of I_x values.

To satisfy the investigators′ curiosity, a last effort was made to achieve some effect on detachment through free-stream turbulence. A horizontal bar of 0.635 cm diam was located 9.5 cm upstream of and parallel to the leading edge at a height such that the wake of the rod impinged on the airfoil at the highest point or "crest" of the airfoil. This did finally cause detachment to move appreciably downstream. However, prior to accepting this as a direct result of free-stream turbulence, per se, the pressure distribution on the airfoil was measured. When the pressure distribution was used with Stratford′s method, it was found that the entire change in x_d was predicted on the basis

of the altered pressure distribution alone. Therefore, it can not be concluded that the gross increase in turbulence, in itself, had any direct effect on x_d. Apparently the beneficial effects of vortex generators are attributable to their being more efficient in redirection of higher-speed air into the inner boundary layer than the less-ordered turbulence of the transverse rod. In either case, the indirect influence on pressure distribution arising from altered boundary layer profiles should not be overlooked.

Prandtl's mixing length concept and the relationship of mixing length to viscous shear stress are well known. (See, e.g., ref. 30). For 2-dimensional, parallel flow, this relation may be expressed as

$$\tau = \rho \ell^2 \left| dU/dy \right| (dU/dy) \qquad (10)$$

where τ = shear stress

and ℓ = mixing length

von Karman's equation for mixing length is (cf. ref. 30)

$$\ell = \kappa \left| (dU/dy)/d^2U/dy^2 \right| \qquad (11)$$

It has been found experimentally that $\kappa \approx 0.4$. Hence, for typical turbulent boundary layers, mixing length is essentially proportional to y within the inner part of the boundary layer.

Prandtl likens ℓ to the mean free path of kinetic theory of gases. In the development of an equation for the mean free path for perfectly elastic, spherical molecules of rarefied gases, it is found that (ref. 31)

$$\lambda \approx 1/(N\sigma) \qquad (12)$$

where λ = mean free path

N = number of molecules per unit volume

σ = effective cross sectional area of molecules

Now stretching this obviously simplified model to accommodate mixing length and mean free path concepts, one may visualize "turbulent lumps" of a diameter proportional to integral scale interacting according to the mixing length and mean free path concepts. Then, N could be regarded as the counterpart of $1/I_x^3$ and σ as the counterpart of I_x^2. If mixing length is analogous to mean free path, it follows from Eqs. (10-12) that ℓ and I_x should have similar distributions with y in the inner part of the boundary layer. The distributions of $I_x(y)$ in Figs. 26 and 29 seem to support this argument. It has to be remembered that local mean velocity U(y) is used with the integrated correlation coefficient (Eq. 4) to obtain I_x, so it is not surprising that I_x tends to zero as the solid surface is approached. Obtaining I_x in this way probably leads to some inaccuracy very near to the wall where $T'(y)$ is relatively large.

In this connection, values of I_x at or just beyond the outer edge of the boundary layer do not necessarily equal the free-stream values because the local mean velocity may be greater or less than the free-stream value. In Fig. 26, $U_e = 1.13\ U_\infty$, and in Fig. 29, $U_e = 0.96\ U_\infty$. Thus, the integral scales are seen to be approximately $I_x = I_{x\infty}\ (U_e/U_\infty)$ when $y \geq \delta$.

CONCLUSIONS

It has been learned that neither a 20-fold increase in free-stream relative turbulence intensity nor a variation of free-stream integral scales produced a significant change in boundary layer detachment location on the subsonic airfoil studied. The integral scales were on the order of boundary layer total thickness, and data were obtained in which turbulence intensity and integral scale were varied independently. A turbulent boundary layer was maintained upstream of the separation zone. All intermediate experimental data, such as the influence of turbulence intensity upon skin friction coefficient, agree in all essentials with results published by others.

The penetration of free-stream turbulence into the turbulent boundary layer was also investigated in an effort to shed light on the lack of influence of free-stream turbulence properties on boundary layer detachment. Results presented herein clearly show how velocity, turbulence intensity, and integral scale profiles were affected when the latter two parameters were varied in the free stream. In this experiment, the velocity profiles are not affected, but the intensity and scale profiles clearly show interaction with the free stream. Despite the consistent and plausible evidence of the expected penetration of turbulence, under the conditions of this research, this interaction did not change x_d to any major degree. Such a change in x_d only occurred

when a gross increase in free-stream turbulence was brought about by placing a bluff obstacle immediately upstream of the airfoil, and it appears that the effect on x_d actually should be credited to the altered pressure distribution that accompanied the much thickened boundary layer.

It is shown that the influence of free-stream turbulence diminished as the airfoil surface was approached. This lessened effect near the surface, plus the weak influence of C_f on x_d and the dominance of pressure gradient seems to account for the insensitivity of x_d to the free-stream turbulence characteristics as long as the boundary layer character and thickness distribution is unchanged.

When Stratford's procedure for predicting x_d was used in conjunction with the measured pressure distributions and the computational modification presented by Cebeci, et al., very good agreement with measured x_d resulted.

ACKNOWLEDGMENTS

This work was performed at Vanderbilt University with the aid of NASA Research Grant NAG-1-483. The NASA Technical Officer was W. D. Harvey, Langley Research Center. That support is sincerely appreciated. The investigators also owe thanks to the School of Engineering and, particularly, to the Department of Mechanical and Materials Engineering for support in this research.

Several former and current associates who contributed to the planning, preparation, and collection of data for this study deserve recognition for their valued assistance. These are

W. R. Seebaugh

Rajiv B. Gokhale

G. Gregory Harris

Barry Batista

REFERENCES

1. Hancock, P.E.: Effect of Free-Stream Turbulence on Turbulent Boundary Layers. Ph.D. Thesis, Imperial College, University of London, 1978.

2. Meier, H. U.: The Response of Turbulent Boundary Layers to Small Turbulence Levels in the External Free Stream. ICAS Paper No. 76-05, The Tenth Congress of the International Council of the Aeronautical Sciences, Oct. 1976.

3. Simonich, J. C. and Bradshaw, P.: Effect of Free-Stream Turbulence on Heat Transfer Through a Turbulent Boundary Layer. ASME Journal of Heat Transfer, vol. 100, Nov. 1978. pp. 671 - 677.

4. Meier, H. U. and Kreplin, H.- P.: Influence of Freestream Turbulence on Boundary-Layer Development. AIAA Journal, vol. 18, Jan. 1980, pp. 11 - 15.

5. Hancock, P. E. and Bradshaw, P.: The Effect of Free-Stream Turbulence on Turbulent Boundary Layers. ASME Journal of Fluids Engineering, vol. 105, Sept. 1983, pp. 284 - 289.

6. Blair, M. F.: Influence of Free-Stream Turbulence on Turbulent Boundary Layer Heat Transfer and Mean Profile Development, Part 1 - Experimental Data and Part 2 - Analysis of Results. ASME Journal of Heat Transfer, vol. 105, Feb. 1983, pp. 33 - 47.

7. Castro, T. P.: Effects of Free-Stream Turbulence on Low Reynolds Number Boundary Layers. ASME Journal of Fluids Engineering, vol. 106, Sept. 1984, pp. 298 - 306.

8. Townsend, A. A.: The Behaviour of a Turbulent Boundary Layer Near Separation. Journal of Fluid Mechanics, Vol. 12, April 1962, pp. 536 - 554.

9. Fisher, C. E.: Autocorrelation and the Integral Scale in Grid Induced Turbulent Flow. M. S. Thesis, Vanderbilt University, 1985.

10. Gokhale, R. B.: An Investigation of the Dissipation Length Parameter of Turbulence in an Open Circuit Wind Tunnel.

M. S. Thesis, Vanderbilt University, 1986.

11. Harris, G. G.: Experimental Study of Laminar Separation Bubbles on an Airfoil in Subsonic Flow. M. S. Thesis, Vanderbilt University, 1986.

12. Potter, J. L.: Transition from Laminar to Turbulent Flow in Separated Shear Layers. Submitted to AIAA Journal, 1986.

13. Simpson, R. L.: A Review of Some Phenomena in Turbulent Flow Separation. ASME Journal of Fluids Engineering. vol. 103, Dec. 1981, pp. 520 - 533.

14. Bradshaw, P.: An Introduction to Turbulence and Its Measurement, Pergamon Press, Oxford, 1971.

15. Townsend, A. A.: Structure of Turbulent Shear Flow. University Press, Cambridge, 1956.

16. Hinze, J. O.: Turbulence. McGraw-Hill, New York, 1959.

17. Dryden, H. L.; Schubauer, G. B.; Mock, W. C., Jr.; and Skramstad, H. K.: Measurements of Intensity and Scale of Wind-Tunnel Turbulence and their Relation to the Critical Reynolds Number of Spheres. NACA Report No. 581, 1937.

18. Bradshaw, P.: Effect of Free-Stream Turbulence on Turbulent Shear Layers. Imperial College of Science and Technology I. C. Aero Report 74-10, Oct. 1974. Also ARC-35648, 1974.

19. Schlichting, H.: Boundary Layer Theory. McGraw-Hill Book Co., New York, 1960, 4th ed., pp. 30 - 31.

20. Willis, J. A. B.: The Correction of Hot-Wire Readings for Proximity to a Solid Boundary. Journal of Fluid Mechanics, vol. 12, Mar. 1962, pp. 388 - 396.

21. Patel, V. C.: Calibration of the Preston Tube and Limitation on Its Use in Pressure Gradients, Journal of Fluid Mechanics, vol. 23, 1965, pp. 185 - 208.

22. Frei, D. and Thomann, H.: Direct Measurements of Skin Friction in a Turbulent Boundary Layer With a Strong Adverse Pressure Gradient. Journal of Fluid Mechanics, vol. 101, 1980, pp. 79 - 95.

23. Tan-atichat, J.; Nagib, H. M.; and Drubka, R. E.: Effect of Axisymmetric Contractions on Turbulence of Various Scales. Illinois Institute of Technology Report N80-32382, Sept. 1980.

24. Owen, F. K.; Stainback, P. C.; and Harvey, W. D.: An Evaluation of Factors Affecting the Flow Quality in Wind Tunnels. AGARD-CP-348, 1983.

25. Uberoi, Mahinder S.: Effect of Wind Tunnel Contraction on Free-Stream Turbulence. Journal of the Aeronautical Sciences, vol. 23, no. 8, Aug. 1956, pp. 754 - 764.

26. Chehroudi, B. and Simpson, R. L.: Space-Time Results for a Separating Turbulent Boundary Layer Using a Rapidly Scanning Laser Anemometer. Journal of Fluid Mechanics, vol. 160, 1985, pp. 77 - 91.

27. Stratford, B. S.: The Prediction of Separation of the Turbulent Boundary Layer. Journal of Fluid Mechanics, vol. 5, 1959, pp. 1 - 16.

28. Cebeci, T.; Mosinskis, G. J.; and Smith, A. M. O.: Calculation of Separation Points in Incompressible Turbulent Flows. AIAA Journal of Aircraft, vol. 9, Sept. 1972, pp. 618 - 624.

29. Hahn, M.; Rubbert, P.; and Mahal, A.: Evaluation of Separation Criteria and their Application to Separated Flow Analysis. Air Force Flight Dynamics Laboratory/FXM, AFSC, AFFDL-TR-72-145, Jan. 1973. (AD757531)

30. Prandtl, L.: The Mechanics of Viscous Fluids, in Aerodynamic Theory, III, W. F. Durand, ed., California Institute of Technology, 1943.

31. Present, R. D.: Kinetic Theory of Gases. McGraw-Hill, 1958.

APPENDIX I

DATA COLLECTION AND REDUCTION PROGRAMS

The following programs were written and used to collect turbulent velocity data and to calculate the turbulence intensity, integral scale, and dissipation length parameter from the raw data. The purpose of each program and its listing is included. The comments in each program describe its operation.

A. GETSLOWDATA

This BASIC program for the APPLE IIe computer is used as indicated in Appendix II to collect the basic velocity data needed to calculate the turbulence intensity and integral scale. The assembly language subroutine FASTER.OBJ is the actual data collection routine.

```
10  HOME : CLEAR : HIMEM: 38144
20  DIM A%(15200),B%(500)
30 R% = 15000:M% = 384:MTIME = 54:CTIME = 10:MICRO = 1E06
40 DM = 6000:BFS = 5000:BIG% = 4096:G1 = 0
50  VTAB 5: HTAB 5: PRINT "LOADING MACHINE LANGUAGE SUBROUTINE "
60 D$ =  CHR$ (4): PRINT D$;"BLOAD MONDELAY.OBJ,A$9500"
70  HOME : VTAB 5: HTAB 10: PRINT "CHANNEL NUMBER";: HTAB 30: PRINT "INPUT
    "
80  HTAB 16: PRINT "0";: HTAB 31: PRINT "RMS": HTAB 15: PRINT "15";: HTAB
    31: PRINT "MKS": VTAB 11: HTAB 20: PRINT "RANGE";: HTAB 30: PRINT "CO
    DE"
90  HTAB 18: PRINT "0 - 5 V";: HTAB 32: PRINT "0": HTAB 18: PRINT "0 - 1 V
    ";: HTAB 32: PRINT "1": HTAB 17: PRINT "0 - .5 V";: HTAB 32: PRINT "2
    ": HTAB 17: PRINT "0 - .1 V";: HTAB 32: PRINT "3": HTAB 5: PRINT "ADD
     4 TO GAIN CODE FOR BIPOLAR RANGE"
100  PRINT : PRINT : INPUT "INPUT GAIN FOR CHANNEL #0 ";G0:C0G% = 0 + 16 *
    G0:C1G% = 15 + 16 * G1
110  POKE 6,C0G%: POKE 7,C1G%
120  HOME : PRINT  CHR$ (7): VTAB 15
130  INPUT "SAMPLE TIME? (SEC) ";TIME
140  INPUT "NUMBER OF SAMPLES? ";NA%: IF NA% <  = R% GOTO 160
150  PRINT "MAXIMUM SAMPLES EXCEEDED": PRINT R%;" SAMPLES TAKEN ":NA% = R%

160 DR = TIME / NA% * MICRO: IF DR < MTIME GOTO 180
170 DA = (DR - MTIME) / CTIME:AH% =  INT (DA / 256):AL% = DA - AH% * 256: GOTO
    190
180 AH% = 0:AL% = 0
190 SPACE = ((AH% * 256 + AL%) * CTIME + MTIME) / 1000:DR = SPACE * 1000
195  PRINT : PRINT : PRINT "TIME BETWEEN SAMPLES = ";SPACE;" msec"
200 DB = (DM - MTIME) / CTIME:BH% =  INT (DB / 256):BL% = DB - BH% * 256
210  POKE 64,AH%: POKE 65,AL%: POKE 66,BH%: POKE 67,BL%
220 A%(0) = NA% / 128 + 1:B%(0) = 3
230  PRINT : PRINT : INPUT "READY TO SAMPLE ? ";G0$
240  POKE 8,1
250  CALL 38144
260 BSUM = 0
270  FOR I = 1 TO M%:BSUM = BSUM + B%(I): NEXT
280 BAVG = BSUM / M%
290 BVOLT = BAVG * BFS / BIG%
300  PRINT : PRINT "MKS VOLTAGE = ";BVOLT;" mV":BVOLT = BVOLT / 1000
310  PRINT : PRINT : PRINT : INPUT "SAVE DATA? (ENTER 1 FOR YES, 0 FOR NO)
     ";G0%
320  IF G0% < 1 GOTO 480
330  HOME : VTAB 22: INPUT "ENTER DATA FILE NAME ";F$
340  INPUT "DISK DRIVE NUMBER ? ";A$
350  PRINT : PRINT : INPUT "DC VOLTAGE = ? (mV) ";VDC
355  CALL 38288
360 CD$ = ",D":N$ = F$ + CD$ + A$
370  PRINT : HTAB 10: PRINT "SAVING ";F$
380  PRINT D$;"OPEN ";N$
390  PRINT D$;"WRITE ";F$
400  PRINT NA%
410  PRINT G0
420  PRINT DR
430  PRINT BVOLT
440  PRINT VDC
450  FOR I = 1 TO NA%: PRINT A%(I): NEXT
470  PRINT D$;"CLOSE ";F$
480  HOME : VTAB 15: INPUT "ANOTHER RUN? (1--YES;0--NO) ";SB%: IF SB% >  =
    1 GOTO 120
490  PRINT "END OF SAMPLING PROGRAM": END
```

```
9500-  18          CLC
9501-  A0 02       LDY   #$02
9503-  B1 6B       LDA   ($6B),Y
9505-  65 6B       ADC   $6B
9507-  85 3A       STA   $3A
9509-  C8          INY
950A-  B1 6B       LDA   ($6B),Y
950C-  65 6C       ADC   $6C
950E-  85 3B       STA   $3B
9510-  A5 6B       LDA   $6B
9512-  85 4A       STA   $4A
9514-  A5 6C       LDA   $6C
9516-  85 4B       STA   $4B
9518-  A5 40       LDA   $40
951A-  85 18       STA   $18
951C-  A5 41       LDA   $41
951E-  85 19       STA   $19
9520-  A5 06       LDA   $06
9522-  85 09       STA   $09
9524-  20 40 95    JSR   $9540
9527-  18          CLC
9528-  A5 3A       LDA   $3A
952A-  85 4A       STA   $4A
952C-  A5 3B       LDA   $3B
952E-  85 4B       STA   $4B
9530-  A5 42       LDA   $42
9532-  85 18       STA   $18
9534-  A5 44       LDA   $44
9536-  85 19       STA   $19
9538-  A5 07       LDA   $07
953A-  85 09       STA   $09
953C-  20 40 95    JSR   $9540
953F-  60          RTS
9540-  A0 08       LDY   #$08
9542-  B1 4A       LDA   ($4A),Y
9544-  85 05       STA   $05
9546-  A9 09       LDA   #$09
9548-  18          CLC
9549-  65 4A       ADC   $4A
954B-  85 5A       STA   $5A
954D-  A9 00       LDA   #$00
954F-  65 4B       ADC   $4B
9551-  85 5B       STA   $5B
9553-  A0 00       LDY   #$00
9555-  A6 09       LDX   $09
9557-  8E D0 C0    STX   $C0D0
955A-  A5 18       LDA   $18
955C-  85 1B       STA   $1B
955E-  A5 19       LDA   $19
9560-  85 1A       STA   $1A
9562-  A5 1A       LDA   $1A
9564-  F0 04       BEQ   $956A
9566-  C6 1A       DEC   $1A
9568-  D0 F8       BNE   $9562
956A-  A5 1B       LDA   $1B
956C-  F0 07       BEQ   $9575
956E-  C6 1B       DEC   $1B
9570-  C6 1A       DEC   $1A
9572-  4C 62 95    JMP   $9562
9575-  AD D1 C0    LDA   $C0D1
```

```
9578-  A6 09       LDX   $09
957A-  91 5A       STA   ($5A),Y
957C-  C8          INY
957D-  AD D0 C0    LDA   $C0D0
9580-  8E D0 C0    STX   $C0D0
9583-  91 5A       STA   ($5A),Y
9585-  C8          INY
9586-  D0 D2       BNE   $955A
9588-  E6 5B       INC   $5B
958A-  C6 05       DEC   $05
958C-  D0 CC       BNE   $955A
958E-  60          RTS
958F-  00          BRK
9590-  A0 08       LDY   #$08
9592-  B1 6B       LDA   ($6B),Y
9594-  85 05       STA   $05
9596-  A9 0B       LDA   #$0B
9598-  18          CLC
9599-  65 6B       ADC   $6B
959B-  85 5A       STA   $5A
959D-  A9 00       LDA   #$00
959F-  65 6C       ADC   $6C
95A1-  85 5B       STA   $5B
95A3-  C8          INY
95A4-  B1 6B       LDA   ($6B),Y
95A6-  85 45       STA   $45
95A8-  C8          INY
95A9-  B1 6B       LDA   ($6B),Y
95AB-  85 44       STA   $44
95AD-  A0 00       LDY   #$00
95AF-  B1 5A       LDA   ($5A),Y
95B1-  85 43       STA   $43
95B3-  C8          INY
95B4-  B1 5A       LDA   ($5A),Y
95B6-  85 42       STA   $42
95B8-  A5 42       LDA   $42
95BA-  38          SEC
95BB-  E5 44       SBC   $44
95BD-  85 40       STA   $40
95BF-  A5 43       LDA   $43
95C1-  E5 45       SBC   $45
95C3-  85 41       STA   $41
95C5-  A5 43       LDA   $43
95C7-  85 45       STA   $45
95C9-  A5 42       LDA   $42
95CB-  85 44       STA   $44
95CD-  88          DEY
95CE-  A5 41       LDA   $41
95D0-  91 5A       STA   ($5A),Y
95D2-  C8          INY
95D3-  A5 40       LDA   $40
95D5-  91 5A       STA   ($5A),Y
95D7-  C8          INY
95D8-  D0 D5       BNE   $95AF
95DA-  E6 5B       INC   $5B
95DC-  C6 05       DEC   $05
95DE-  D0 CF       BNE   $95AF
95E0-  60          RTS
95E1-  D0 C0       BNE   $95A3
95E3-  91 5A       STA   ($5A),Y
95E5-  C8          INY
95E6-  D0 D2       BNE   $95BA
95E8-  E6 5B       INC   $5B
95EA-  C6 05       DEC   $05
95EC-  D0 CC       BNE   $95BA
95EE-  60          RTS
```

B. FIXX.FOR

FIXX is the FORTRAN program which takes the modified data from the APPLE IIe data collection program and restores it to the full data set by a successive addition process. The output data set is used by the following programs AUTOCO and FOURIE.

```
C
C                       PROGRAM FIXX.FOR
C
C
C       THIS PROGRAM READS IN THE MODIFIED A/D VOLTAGE NUMBERS
C       AND RECREATES THE ORIGINAL DATA FILE FOR PROCESSING BY
C       EITHER AUTOCO.FOR OR FOURIE.FOR
C
        DIMENSION NPUT(20000)
        READ(1,*)NPTS
        WRITE(22,*)NPTS
        READ(1,*)IGAIN
        WRITE(22,*)IGAIN
        READ(1,*)DT
        WRITE(22,*)DT
        READ(1,*)VMKS
        WRITE(22,*)VMKS
        READ(1,*)VDC
        WRITE(22,*)VDC

C
C       THE FIRST VOLTAGE NUMBER IS UNMODIFIED.
C
        READ(1,20)NPUT(1)
        WRITE(22,20)NPUT(1)

        DO 40 I = 2,NPTS
        J = I-1
        READ(1,20,ERR=50)IX
20      FORMAT(I6)
        NPUT(I) = IX + NPUT(J)
        WRITE(22,20)NPUT(I)
40      CONTINUE
50      STOP
        END
```

C. AUTOCO.FOR

This FORTRAN program is used on the DEC 1099 computer to convert the raw velocity data collected on the APPLE IIe computer to a more usable form. The output of this program is the integral scale and the turbulence intensity.

```
C                PROGRAM AUTOCO.FOR
C
C
C       THIS PROGRAM TAKES THE RE-CONSTITUTED DATA COLLECTED
C       BY THE APPLE COMPUTER TO PERFORM THE AUTOCORRELATION
C       AND CALCULATE THE INTEGRAL SCALE.
C
        IMPLICIT DOUBLE PRECISION (A-H,O-Z)
        DIMENSION VELOC(20000),RV(500),T(500)
C
C       XMAX IS THE FULL SCALE RANGE OF THE A/D CONVERTER
C
        XMAX = 4096.

        WRITE(6,8)
8       FORMAT(/5X,'NUMBER OF PASSES ? ')
C
C       SET THE MAXIMUM NUMBER OF TIME STEPS TO TAKE.  MUST BE
C       LESS THAN NPTS/2
C
        READ(5,*)NPASS
        WRITE(6,12)
C
C       INPUT THE CALIBRATION COEFFICIENTS USED TO CONVERT
C       FROM VOLTAGE TO VELOCITY
C
12      FORMAT(/5X,'INPUT VELOCITY CORRELATION COEFF''S',/2X,'A = ? ')
        READ(5,*)A
        WRITE(6,13)
13      FORMAT(2X,'B = ? ')
        READ(5,*)B

        READ(1,*)NPTS
        READ(1,*)IGAIN

C
C       DETERMINE THE FULL SCALE VOLTAGE USED ON THE A/D
C
        IF(IGAIN.EQ.0.OR.IGAIN.EQ.4) FS = 5000.
        IF(IGAIN.EQ.1.OR.IGAIN.EQ.5) FS = 1000.
        IF(IGAIN.EQ.2.OR.IGAIN.EQ.6) FS =  500.
        IF(IGAIN.EQ.3.OR.IGAIN.EQ.7) FS =  100.
C
C       IF A BIPOLAR RANGE WAS SELECTED, REDUCE THE RESOLUTION
C       BY HALF.  THIS ALSO SETS THE ZERO AT HALF-SCALE.
C
        IF(IGAIN.GT.3)XMAX = 2048.

        READ(1,*)DT
        READ(1,*)VMKS
        READ(1,*)VDC

C
C       CALCULATE THE WIND TUNNEL MEAN VELOCITY FROM A
C       CONSIDERATION OF THE DYNAMIC PRESSURE AND THE MEASURED
C       VOLTAGE FROM THE MKS PRESSURE TRANSDUCER.
C
        A1 = 1.049*VMKS
        B1 = .030011*(VMKS**0.999708)
        C = 531.*(A1 - B1)
        D = 29.6*2.54
        E = D - A1
        F = (C/E)**0.5
        U = 58.582*F
```

```
C
C       IF THE ANEMOMETER DC VOLTAGE IS LESS THAN 3.1 VOLTS
C       THEN THE PROBE WAS IN THE LOW SPEED SECTION.  CORRECT
C       THE MEAN VELOCITY AS MEASURED BY THE MKS ACCORDINGLY.
C
        IF (VDC.LE.3100.)U = U*0.149

        WRITE(6,14)
14      FORMAT(1H1,10X,60(1H*))
        WRITE(6,15)U
15      FORMAT(/24X,'MKS VELOCITY = ',F10.4,' FT/SEC ')

C
C       READ IN THE A/D VOLTAGE NUMBERS AND CONVERT TO A VOLTAGE
C
        DO 25 I = 1,NPTS
        READ(1,20,ERR=30)IX
20      FORMAT(1G)
        X = FLOAT(IX)
        IF(IGAIN.LE.3)GO TO 24
C
C       CORRECT FOR A BIPOLAR RANGE
C
        X = X - XMAX
24      VELOC(I) = X*FS/XMAX
        SUM = SUM + VELOC(I)
25      CONTINUE
        GO TO 40
30      NPTS = I
C
C       CALCULATE THE AVERAGE VOLTAGE.  IF NOT ZERO, SUBTRACT
C       FROM EACH VOLTAGE.
C
40      VAVG = SUM/FLOAT(NPTS)

        SUM = 0.
        DO 50 I = 1,NPTS
        VDIFF = VELOC(I) - VAVG
C
C       ADD EACH ZERO-BASED VOLTAGE TO THE MEASURED DC VOLTAGE
C       AND CONVERT TO VELOCITY USING CORRELATION COEFFICIENTS.
C
        VOLT = (VDC + VDIFF)/1000.
        VELOC(I) = A*(VOLT**B)
50      SUM = SUM + VELOC(I)
        VAVG = SUM/FLOAT(NPTS)

C
C       CALCULATE THE RMS VOLTAGE TO GET THE INTENSITY
C
        SUM = 0.
        DO 60 I = 1,NPTS
        SUM = SUM + (VELOC(I) - VAVG)**2.
        VELOC(I) = VELOC(I) - VAVG
60      CONTINUE
        VRMS = SQRT(SUM/FLOAT(NPTS))
        TI = VRMS/VAVG*100.

C
C       PERFORM THE AUTOCORRELATION ON THE FLUCTUATING
C       COMPONENTS OF THE VELOCITY.
C
        DO 90 I = 1,NPASS
        SUM = 0.
        DO 70 J = 1,NPTS-(I-1)
        SUM = SUM + VELOC(J)*VELOC(J+I-1)
70      PT = FLOAT(J)
```

```
C
C       RV IS THE AUTOCORRELATION COEFFICIENT
C
        RV(I) = (SUM/FT)/(VRMS*VRMS)
        T(I) = DT*FLOAT(I-1)
C
C       END THE PROCEDURE IF RV(I) IS LESS THAN ZERO:
C
        IF(RV(I).LT.0.)GO TO 95
        WRITE(21,80) T(I),RV(I)
80      FORMAT(2X,F12.6,5X,F12.6)
90      CONTINUE
        GO TO 98

95      NPASS = I
        RV(NPASS) = 0.
        WRITE(21,80)T(NPASS),RV(NPASS)
        WRITE(6,96)NPASS
96      FORMAT(/15X,'NEGATIVE CORRELATION AFTER ',I2,' STEPS')
        WRITE(6,97)T(NPASS)
97      FORMAT(15X,'LAST STEP WAS ',F9.3,' MICROSECONDS')

C
C       THE INTEGRAL SCALE IS FOUND BY USING SIMPSON'S RULE
C       TO INTEGRATE THE AREA UNDER THE RV VS. T CURVE
C
98      H = DT*1.0E-06
        SINT = 0.
        DO 100 I = 2,NPASS-1
100     SINT = SINT + RV(I)
        TSUM = H*SINT + (H/2.)*(RV(1) + RV(NPASS))

        WRITE(6,105)VAVG,VRMS
105     FORMAT(//24X,'AVERAGE VELOCITY = ',F12.5,' FT/SEC',/26X
     C ,'RMS VELOCITY = ',F12.5,' FT/SEC')
        WRITE(6,108)TI

108     FORMAT(27X,'TURBULENCE INTENSITY = ',F6.3,' % ')
        WRITE(6,110)TSUM
110     FORMAT(//29X,'INTEGRAL = ',1PE12.5,' SEC')
        VSUM = VAVG*TSUM*12.
        WRITE(6,120)VSUM
120     FORMAT(29X,'INTEGRAL = ',F12.6,' IN.')
        WRITE(6,130)
130     FORMAT(//10X,60(1H*),////)
        STOP
        END
```

D. FOURIE.FOR

This FORTRAN program for use on the DEC 1099 computer executes the Fast Fourier Transform of the raw velocity data collected by the APPLE IIe computer. The output results are used with a plotting program to examine the power spectrum of the data. The IMSL subroutine FFTRC which actually performs the Fast Fourier Transform must be linked to the program during execution using the command

```
EX FOURIE.FOR,PUB:IMSL.REL/SEARCH
```

```
C
C                       PROGRAM FOURIE.FOR
C
C
C       THIS PROGRAM PERFORMS THE FAST FOURIER TRANSFORM OF
C       THE RE-CONSTITUTED DATA FROM THE APPLE COMPUTER.  AN
C       AVERAGING PROCESS IS USED TO SMOOTH THE RESULTS.
C
C       THE IMSL SUBROUTINE FFTRC IS USED TO PERFORM THE FAST
C       FOURIER TRANSFORM.
C
        DIMENSION VEL(10000),STORE(10000),SGK(2000),IWK(1000),WK(1000)
        COMPLEX FC(5001),TEMP

        SMALL = 1.0E-06
        PI = 3.1415927
        XMAX = 4096.
        WRITE(6,10)
C
C       THE NUMBER OF POINTS USED TO FIND THE FFT MUST BE A
C       POWER OF 2.  HERE 2**11 = 2048 WAS USED.
C
10      FORMAT(///5X,'NUMBER OF POINTS?')
        READ(5,*)N

        READ(1,*)NPTS
        READ(1,*)IGAIN

C
C       DETERMINE THE FULL SCALE VOLTAGE RANGE USED ON THE A/D
C
        IF(IGAIN.EQ.0.OR.IGAIN.EQ.4) FS = 5000.
        IF(IGAIN.EQ.1.OR.IGAIN.EQ.5) FS = 1000.
        IF(IGAIN.EQ.2.OR.IGAIN.EQ.6) FS =  500.
        IF(IGAIN.EQ.3.OR.IGAIN.EQ.7) FS =  100.
C
C       IF A BIPOLAR RANGE WAS SELECTED, REDUCE THE RESOLUTION
C       BY HALF.  THIS ALSO SET THE ZERO AT HALF-SCALE.
C
        IF(IGAIN.GT.3)XMAX = 2048.

C
C       DT IS THE TIME BETWEEN EACH SAMPLE. THE RMS VOLTAGE AND
C       THE ANEMOMETER DC VOLTAGE ARE NOT USED HERE.
C
        READ(1,*)DT
        READ(1,*)VRMS
        READ(1,*)VDC

C
C       READ IN THE A/D VOLTAGE NUMBERS AND CONVERT TO A VOLTAGE
C
        SUM = 0.
        DO 25 I = 1,NPTS
        READ(1,20,ERR=30)IX
20      FORMAT(1G)
        X = FLOAT(IX)
        IF(IGAIN.LE.3)GO TO 26
        X = X - XMAX
26      STORE(I) = X*FS/XMAX
        SUM = SUM + STORE(I)
25      CONTINUE
        GO TO 40
30      NPTS = I
```

```
C
C       CALCULATE THE AVERAGE VOLTAGE.  IF NOT ZERO, SUBTRACT
C       FROM EACH VOLTAGE.
C
40      VAVG = SUM/FLOAT(NPTS)

        DO 50 I = 1,NPTS
        STORE(I) = STORE(I) - VAVG
50      CONTINUE

C
C       THE RECORDS USED FOR THE FFT OVERLAP BY 1/2 THE NUMBER
C       OF SAMPLES IN THE RECORD.  THIS GIVES A BETTER AVERAGE.
C
        NOVER = N/2
        NTIMES = 2*(NPTS/N)
        NSTART = 0

        DO 60 I = 1,2000
C
C       ZERO THE ARRAY OF AVERAGED FOURIER COEFFICIENTS
C
60      SGK(I) = 0.

        DO 140 NCOUNT = 1,NTIMES

C
C       MAKE SURE THE RECORD HAS A ZERO AVERAGE.
C
        SUM = 0.
        DO 70 I = 1,N
        VEL(I) = STORE(NSTART +I)
70      SUM = SUM + VEL(I)
        VAVG = SUM/FLOAT(N)

        DO 80 I = 1,N
80      VEL(I) = VEL(I) - VAVG

C
C       USE A HAMMING WINDOW ON THE FIRST AND LAST 10% OF THE
C       RECORD TO REDUCE THE APPEARANCE OF SIDELOBES CAUSED
C       BY A FINITE RECORD LENGTH.
C
        M = N/10
        IFRONT = M
        IBACK = N-M

        DO 100 I = 1,N
        IF(I.GE.IFRONT) GO TO 90
        J = I-1
        VAR = COS(PI*FLOAT(J)/FLOAT(M-1))
        VEL(I) = (VEL(I)/2.)*(1. - VAR)
        GO TO 100
90      IF(I.LE.IBACK) GO TO 100
        J = N-I
        VAR = COS(PI*FLOAT(J)/FLOAT(M-1))
        VEL(I) = (VEL(I)/2.)*(1. - VAR)
100     CONTINUE
```

```
C
C       PERFORM THE FAST FOURIER TRANSFORM ON THE RECORD
C
        CALL FFTRC(VEL,N,FC,IWK,WK)

C
C       AVERAGE EACH DATA POINT IN THE RECORD WITH THE DATA
C       POINTS ON EACH SIDE.
C
        DO 110 I = 2,(N/2)
        TEMP = 0.25*FC(I-1) + 0.5*FC(I) + 0.25*FC(I+1)
110     FC(I) = TEMP/0.875

C
C       NORMALIZE THE COMPLEX FOURIER COEFFICIENTS BY COMPUTING
C       THE ABSOLUTE VALUE AND DIVIDING BY THE NUMBER OF SAMPLES
C       IN THE RECORD.  COMPUTE THE AVERAGE FOR EACH RESULTING
C       FREQUENCY
C
        FREQ = 0.
        GDC = 10.*ALOG10(((CABS(FC(1))**2.)/SMALL)/FLOAT(N/2))
        SGK(1) = SGK(1) + GDC

        J = N/2
        NSTEP = J/1000
        IF(NSTEP.LE.1) NSTEP = 1
        DF = 1./(2.*FLOAT(J)*(SMALL*DT))
        NGK = 1

        DO 130 I = 1,(J/NSTEP)
        IGK = I + 1
        FSUM = 0.
        GSUM = 0.
        DO 120 L = 1,NSTEP
        FREQ = FREQ + DF
        NGK = NGK + 1
        GK = 10.*ALOG10(((CABS(FC(NGK))**2.)/SMALL)/FLOAT(J))
        FSUM = FSUM + FREQ
        GSUM = GSUM + GK
120     CONTINUE
        GAVG = GSUM/FLOAT(NSTEP)
        SGK(IGK) = SGK(IGK) + GAVG
130     CONTINUE
        NSTART = NSTART + NOVER

140     CONTINUE

C
C       OUTPUT THE AVERAGED FREQUENCIES AND NORMALIZED
C       SPECTRUM AT THAT FREQUENCY IN DB.
C
        FREQ = 0.
        DO 150 I = 1,(J/NSTEP)
        GAVG = SGK(I)/FLOAT(NTIMES)
        WRITE(22,*)FREQ,GAVG
        FREQ = FREQ + DF*(FLOAT(NSTEP))
150     CONTINUE

        STOP
        END
```

E. REDUCE.FOR

REDUCE.FOR for the DEC 1099 computer takes the data produced by AUTOCO.FOR for one velocity and all grid positions and calculates the correlations for the integral scale and turbulence intensity. It also calculates the dissipation length parameter by using the turbulence decay law proposed by Castro. A nonlinear optimization method is used to find the virtual origin which gives the best power-function fit to the integral scale results.

```
C
C                       PROGRAM REDUCE.FOR
C
C       THIS PROGRAM TAKES THE GRID POSITION, INTEGRAL SCALE,
C       AND TURBULENCE INTENSITY DATA AT ONE MEAN VELOCITY AND
C       PERFORMS A CORRELATION FOR THE INTEGRAL SCALE AND
C       THE DISSIPATION LENGTH PARAMETER.
C
        IMPLICIT DOUBLE PRECISION (A-H,O-Z)
        DOUBLE PRECISION NAME
        DIMENSION XGRID(20),TSCALE(20),XSCALE(20),TPRIME(20),XM(20)
        DIMENSION X(20),Y(20),XD(20),YD(20)
        COMMON /X/X/XSCALE/XSCALE/AX/AX/BX/BX/RX/RX/NPTS/NPTS

        T104 = 1.0E-04
        VISC = 15.69E-06
        NAME = 'SMALL'
        READ (1,*)NPTS
        READ (1,*)XMESH,B
        READ (1,*)XPROBE
        READ (1,*)SPEED
        IF(SPEED.LT.20.)NAME = 'LARGE'

        DO 10 I = 1,NPTS
        READ(1,*)XGRID(I),TSCALE(I),TPRIME(I)
10      CONTINUE

C
C       SORT THE DATA IN ORDER BY GRID POSITION
C
        XN = FLOAT(NPTS)
        ND = 2**(ALOG(XN)/ALOG(2.)) - 1
20      DO 60 I = 1,(NPTS-ND)
        IF(XGRID(I).LE.XGRID(I+ND)) GO TO 60
        TX = XGRID(I+ND)
        TLT = TSCALE(I+ND)
        TTURB = TPRIME(I+ND)
        XGRID(I+ND) = XGRID(I)
        TSCALE(I+ND) = TSCALE(I)
        TPRIME(I+ND) = TPRIME(I)
        IF(I.GT.ND) GO TO 30
        XGRID(I) = TX
        TSCALE(I) = TLT
        TPRIME(I) = TTURB
        GO TO 60
30      DO 40 J = (I-ND),1,(-ND)
        IF(TX.GE.XGRID(J)) GO TO 50
        XGRID(J+ND) = XGRID(J)
        TSCALE(J+ND) = TSCALE(J)
40      TPRIME(J+ND) = TPRIME(J)
50      XGRID(J+ND) = TX
        TSCALE(J+ND) = TLT
        TPRIME(J+ND) = TTURB
60      CONTINUE
        ND = ND/2
        IF(ND.GT.0)GO TO 20
```

```
C
C       CALCULATE THE INTEGRAL SCALE FROM THE TIME SCALE DATA
C       CALCULATE THE TURBULENT ENERGY DECAY (U**2)/(U'**2)
C
        DO 70 I = 1,NPTS
        X(I) = XGRID(I) - XPROBE
        XM(I) = X(I)/XMESH
        XSCALE(I) = (TSCALE(I)*T104*SPEED)*100.
        Y(I) = (TPRIME(I)/100.)**2.
        YD(I) = 1./Y(I)
70      CONTINUE

C
C       FIND THE DISSIPATION VIRTUAL ORIGIN BY A LINEAR FIT OF
C       THE TURBULENCE DECAY DATA
C
        CALL LFUNC(X,YD,AL,BL,RL,NPTS)

        XOD = -AL/BL
        DO 71 I = 1,NPTS
71      XD(I) = (X(I) - XOD)/XMESH

C
C       DO A POWER FUNCTION FIT TO THE TURBULENCE DECAY DATA
C       USING THE VIRTUAL ORIGIN TO GET THE COEFFICIENTS USED
C       TO CALCULATE THE DISSIPATION PARAMETER.
C
        CALL PFUNC(XD,Y,AD,BD,RD,NPTS)
        CALL PFUNC(X,TPRIME,AT,BT,RT,NPTS)

C
C       USE A UNIVARIATE LINE SEARCH ALGORITHM TO FIND THE BEST
C       FIT TO THE INTEGRAL SCALE DATA USING A VIRTUAL ORIGIN
C
        NVAR = 1
        XO = 0.
        CALL FUNC(XO,FXO,NVAR)
        CALL GRADIE(XO,FXO,PART,NVAR)
        SMAG = SQRT(PART**2.)
        TEST = -PART/SMAG

        CALL GOLDEN(XO,TEST,XORG,NVAR)

        WRITE(6,72)XMESH,NAME
72      FORMAT(1H1,20X,'DATA FOR ',F5.2,' cm GRID IN ',A5
     C ,' TEST SECTION')
        WRITE(6,74)SPEED,XPROBE
74      FORMAT(/33X,'VELOCITY = ',F5.2,' m/s ',/33X,'PROBE AT X = ',
     C F6.2,' cm',//)
        WRITE(6,80),XORG,RX,AX,BX
80      FORMAT(10X,'INTEGRAL SCALE VIRTUAL ORIGIN AT Xo = ',F7.2,' cm',
     C /20X,'R = ',F9.6,/20X,'A = ',1PE12.4,/20X,'B = ',1PE12.4,//)
        WRITE(6,90)XOD,RD,AD,BD
90      FORMAT(10X,'DISSIPATION VIRTUAL ORIGIN AT Xo = ',F7.2,' cm',
     C /20X,'R = ',F9.6,/20X,'A = ',1PE12.4,/20X,'B = ',1PE12.4,//)
        WRITE(6,94)RT,AT,BT
94      FORMAT(10X,'CORRELATION FOR TURBULENCE INTENSITY IS',/20X,
     C 'R = ',F9.6,/20X,'A = ',1PE12.4,/20X,'B = ',1PE12.4,///)
```

```
      WRITE(6,100)
100   FORMAT(//T8,'GRID',T17,'X',T22,'X-Xoi',T29,'X-Xod',T36,'TURB',
     C T45,'TIME',T54,'INT',T63,'DISS',T73,'Lx')
      WRITE(6,110)
110   FORMAT(T6,'POSITION',T16,'---',T22,'-----',T29,'-----',
     C T35,'INTENS',T44,'SCALE',T53,'SCALE',T62,'SCALE',T72,'----')
      WRITE(6,120)
120   FORMAT(T8,'(cm)',T17,'M',T24,'M',T31,'M',T37,'(%)',T45,'(uS)',
     C T54,'(cm)',T63,'(cm)',T73,'Ld',/T4,74(1H=))


      RB = SPEED*B/(100.*VISC)

      DO 140 I = 1,NPTS
      XG = XGRID(I)
      TP = TPRIME(I)
C
C     CALCULATE THE DISSIPATION SCALE USING THE VIRTUAL ORIGIN
C     AND THE POWER-FUNCTION COEFFICIENTS.
C
      DS = (AD**0.5)*XMESH*(XD(I)**(1. + BD/2.))/(-BD)
      XTD = XSCALE(I)/DS
      TM = TSCALE(I)*100.
      XOBR = (X(I) - XORG)/(B*RB)
      YBR = XSCALE(I)/(B)
      WRITE(6,130)XG,XM(I),XOM,XD(I),TP,TM,XSCALE(I),DS,XTD
130   FORMAT(T7,F6.2,T15,F5.2,T21,F6.2,T28,F6.2,T36,F5.3,T43,F7.2,
     C T53,F6.4,T62,F6.4,T71,F6.4)
      WRITE(30,*)X(I),TPRIME(I)
      WRITE(31,*)X(I),XSCALE(I)
      WRITE(32,*)X(I),DS
      WRITE(9,*)XOBR,YBR
140   CONTINUE

      WRITE(6,150)
150   FORMAT(1H1)
      STOP
      END



C
C     GOLDEN IS THE UNIVARIATE LINE SEARCH ALGORITHM WHICH
C     USES THE GOLDEN SECTION BRACKETING TECHNIQUE
C
      SUBROUTINE GOLDEN(X,S,XSTAR,N)
      IMPLICIT DOUBLE PRECISION(A-H,O-Z)

      F1 = 0.381966
      F2 = 0.618034
      STOL = 0.001

      CALL FUNC(X,FX,N)
      FXL = FX
      XL = X

      DO 10 I = 1,800
      XH = XL + S
      CALL FUNC(XH,FXH,N)
      IF(FXH.GT.FXL) GO TO 20
      XL = XH
      FXL = FXH
10    CONTINUE
```

```
20      IF(I.EQ.1) GO TO 30
        XL = XH - 2.*S
        CALL FUNC(XL,FXL,N)

30      DELTA = XH - XL
        DO 60 IB = 1,300
        DEL1 = F1*DELTA
        DEL2 = F2*DELTA
        X1 = XL + DEL1
        X2 = XL + DEL2
        CALL FUNC(X1,FX1,N)
        CALL FUNC(X2,FX2,N)
        IF(FX2.GE.FX1) GO TO 40
        DELTA = XH - X1
        XL = X1
        GO TO 50
40      DELTA = X2 - XL
        XH = X2
50      IF(ABS(DELTA).LE.STOL) GO TO 70
60      CONTINUE

70      XSTAR = X2
        RETURN
        END



C
C       THIS SUBROUTINE IS USED BY GOLDEN AS THE OBJECTIVE FUNCTION
C       THE TASK IS TO MAXIMIZE THE POWER-FUNCTION CORRELATION
C       COEFFICIENT RX BY CHOICE OF THE VIRTUAL ORIGIN X0.
C
        SUBROUTINE FUNC(X0,FX,NVAR)
        IMPLICIT DOUBLE PRECISION (A-H,O-Z)
        DIMENSION Y(20),TRY(20),X(20),XSCALE(20)
        COMMON /X/X/XSCALE/XSCALE/AX/AX/BX/BX/RX/RX/NPTS/NPTS

        DO 10 I = 1,NPTS
        TRY(I) = X(I) - X0
        Y(I) = XSCALE(I)
10      CONTINUE

        CALL PFUNC(TRY,Y,AX,BX,RX,NPTS)

        FX = -(RX)

        RETURN
        END



C
C       PFUNC IS THE POWER-FUNCTION LEAST-SQUARES ANALYSIS FUNCTION
C
        SUBROUTINE PFUNC(X,Y,A,B,R,N)
        IMPLICIT DOUBLE PRECISION (A-H,O-Z)
        DIMENSION X(20),Y(20)
```

```
      TSMALL = 0.000001
      X1 = 0.
      Y1 = 0.
      S1 = 0.
      T1 = 0.
      W1 = 0.
      DO 10 I = 1,N
      IF(X(I).LE.0.)GO TO 2
      XL = DLOG(X(I))
      GO TO 4
2     XL = DLOG(TSMALL)
4     IF(Y(I).LE.0.)GO TO 6
      YL = DLOG(Y(I))
      GO TO 8
6     YL = DLOG(TSMALL)
8     X1 = X1 + XL
      Y1 = Y1 + YL
      S1 = S1 + XL*YL
      T1 = T1 + XL*XL
10    W1 = W1 + YL*YL

      XN = FLOAT(N)
      D1 = XN*T1 - X1*X1
      AL = (Y1*T1 - X1*S1)/D1
      B = (XN*S1 - X1*Y1)/D1
      R = (AL*Y1 + B*S1 - Y1*Y1/XN)/(W1 - Y1*Y1/XN)
      A = DEXP(AL)

      RETURN
      END



C
C     LFUNC IS A LINEAR LEAST-SQUARES ANALYSIS ROUTINE
C
      SUBROUTINE LFUNC(X,Y,A,B,R,N)
      IMPLICIT DOUBLE PRECISION (A-H,O-Z)
      DIMENSION X(20),Y(20)

      X1 = 0.
      Y1 = 0.
      S1 = 0.
      T1 = 0.
      W1 = 0.
      DO 10 I = 1,N
      X1 = X1 + X(I)
      Y1 = Y1 + Y(I)
      S1 = S1 + X(I)*Y(I)
      T1 = T1 + X(I)*X(I)
10    W1 = W1 + Y(I)*Y(I)

      XN = FLOAT(N)
      D1 = XN*T1 - X1*X1
      A = (Y1*T1 - X1*S1)/D1
      B = (XN*S1 - X1*Y1)/D1
      R = (A*Y1 + B*S1 - Y1*Y1/XN)/(W1 - Y1*Y1/XN)

      RETURN
      END
```

```
C
C       GRADIE IS USED TO FIND THE DIRECTION IN WHICH TO BEGIN
C       SEARCHING TO ACHIEVE THE BEST FIT FOR THE INTEGRAL SCALE
C       CORRELATION.
C
        SUBROUTINE GRADIE(X,FX,PART,N)
        IMPLICIT DOUBLE PRECISION (A-H,O-Z)

        DX = 1.0E-04

        X1 = X + DX
        CALL FUNC(X1,FX1,N)
        PART = (FX1 - FX)/DX

        RETURN
        END
```

Test Section	Max. Speed	(Re/L) x 10^{-4}
1.02 x 1.02 m	11.2 m/s	71.3 m^{-1}
(40 x 40 in.)	36.7 fps	1.81 $in.^{-1}$
0.411 x 0.411 m	74.7 m/s	462 m^{-1}
(16.2 x 16.2 in.)	245 fps	11.7 $in.^{-1}$

Table 1.- VUES wind tunnel flow data. Assumed room air at typical conditions of 1.002 x 10^5 N/m^2 (29.60 in.Hg) and 295 K (72°F). No model installed in tunnel.

Grid No./ Grid M cm	Grid X cm	U_∞ m/s	T'_∞ %	$I_{x\infty}$ cm	$L_{x\infty}$ cm
#1/10.16	265.7	25.6	0.45	0.82	0.65
	234.5	25.6	0.53	0.70	0.53
	265.7	50.6	0.57	0.98	0.81
	265.7	71.3	0.63	1.09	0.86
	234.5	50.6	0.66	0.86	0.67
	215.5	25.6	0.70	0.64	0.44
	234.5	71.3	0.74	1.06	0.74
	215.5	71.3	0.85	0.94	0.65
	194.0	25.6	0.87	0.64	0.33
	215.5	50.6	0.88	0.81	0.58
	194.0	50.6	0.99	0.83	0.46
	173.2	25.6	1.01	0.57	0.19
	194.0	71.3	1.02	0.92	0.54
	173.2	50.6	1.16	0.72	0.31
	173.2	71.3	1.18	0.86	0.40
#2/5.08	265.7	25.6	0.22	1.43	0.34
	234.5	25.6	0.22	1.09	0.31
	265.7	50.6	0.26	1.51	0.38
	194.0	25.6	0.28	0.84	0.26
	265.7	71.3	0.31	1.38	0.56
	194.0	50.6	0.1	0.78	0.30
	215.5	71.3	0.32	0.81	0.49
	173.2	25.6	0.32	0.73	0.23
	194.0	25.6	0.37	0.71	0.46
	173.2	50.6	0.38	0.70	0.27
	153.2	25.6	0.38	0.63	0.20
	173.2	71.3	0.40	0.53	0.43
	153.2	50.6	0.46	0.45	0.24
	153.2	71.3	0.48	0.43	0.39
#3/5.08	265.7	26.4	0.45	0.79	
	265.7	47.0	0.46	0.59	
	265.7	64.5	0.50	0.45	
	215.5	26.5	0.60	0.61	
	215.5	51.5	0.66	0.58	
	215.5	62.8	0.74	0.68	
	153.2	26.4	1.08	0.53	
	153.2	50.3	1.19	0.58	
	153.2	64.6	1.17	0.64	
#4/2.54	58.4	25.0	2.59	0.64	
	58.4	49.8	2.73	0.66	
	58.4	55.8	2.73	0.71	
#5/5.08	58.4	52.5	3.16	0.77	
No Grid	----	51.6	0.16	1.35	
	----	65.1	0.34	1.18	

Table 2.- Summary of free-stream turbulence characteristics.

α°	B.L. Tnp	U_∞ m/s	T_∞ %	I_{x_∞} cm	Exp.* x_d	$\delta_{.995}$ cm at x=22.1	$\delta_{.995}$ cm at x=29.7
1	yes	50.5	0.16	1.35	29.6	0.46	0.93
3	yes	"	"	"	29.7	----	----
6	yes	"	"	"	29.1	.60	----
9	yes	"	"	"	27.9	----	----
1	yes	64.2	0.34	1.18	30.2	.44	.88
1	yes	50.5	0.46	0.59	29.7	.46	.93
1	yes	64.2	0.50	0.45	30.4	----	----
1	yes	50.5	1.19	0.58	29.7	.46	.93
1	yes	64.2	1.17	0.64	30.2	----	----
1	yes	49.8	2.73	0.66	29.7	.46	.93
1	yes	51.1	3.16	0.77	30.5	.46	.93
1	no	50.5	0.16	1.35	30.1		
1	no	64.2	0.34	1.18	30.2		

* ± 0.25 cm est.

Table 3.- Detachment locations shown by liquid film and corresponding flow conditions.

$I_x \propto / \delta_{.995}$	T'_∞ %	x_d cm
0.67	0.46	29.7 ± 0.25
"	1.19	" "
"	2.73	" "
0.56	0.31	" "
"	0.38	" "
"	2.85	" "

Table 4.- Effect of free-stream turbulence intensity upon detachment location with constant turbulence integral scale

T'_∞%	$I_x \propto / \delta_{.995}$	x_d cm
0.30	1.64	29.7 ± 0.25
"	1.32	" "
"	1.23	" "
"	0.63	" "

Table 5.- Effect of free-stream integral scale upon detachment location with constant turbulence intensity.

Run	α°	U_∞ m/s	T'_∞%	I_x ∞ cm	x_d cm		
					Exp.*	Strat. 1	Strat. 2
396B	1	50.5	0.16	1.35	29.6	28.3	29.9
404A	3	"	"	"	29.7	27.1	27.7
404B	9	"	"	"	27.9	27.9	27.9
374A	1	"	1.19	0.58	29.7	27.4	30.1
374B	"	64.2	1.17	0.64	30.2	27.7	29.9
363	"	49.8	2.73	0.66	29.7	28.5	28.8
403	"	51.1	3.16	0.77	30.5	28.4	30.0

*Uncertainty ± 0.25 cm

Table 6.- Comparison of experimental and predicted detachment locations

Run	x_d cm		
	Exp.	Strat.2	Townsend
396B	29.6	29.9	30.8
404A	29.7	27.7	28.7
374A	29.7	30.1	30.8
363	29.7	28.8	29.26
403	30.5	30.0	30.7

Table 7.- Comparison of two prediction methods

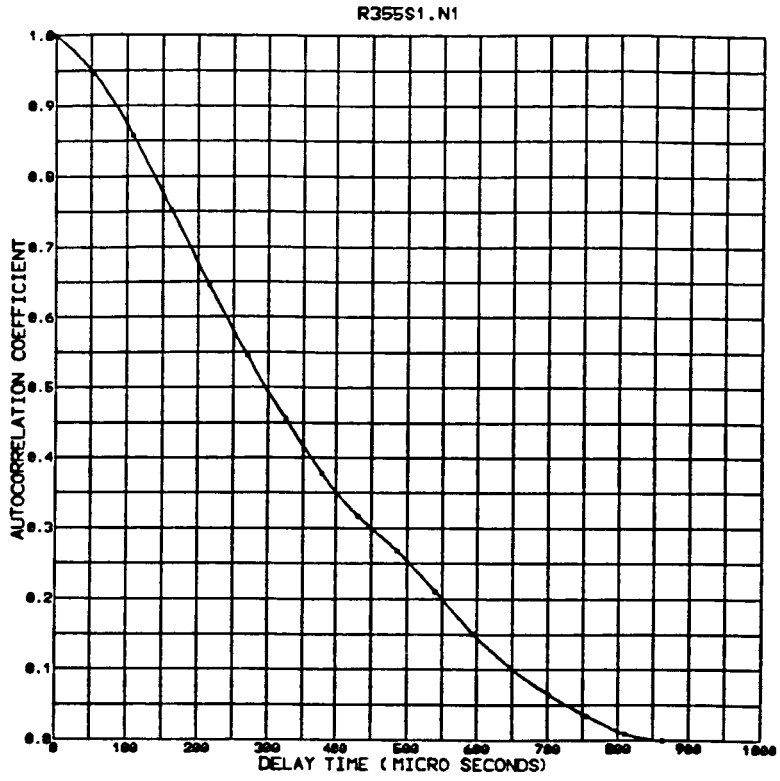

(a)

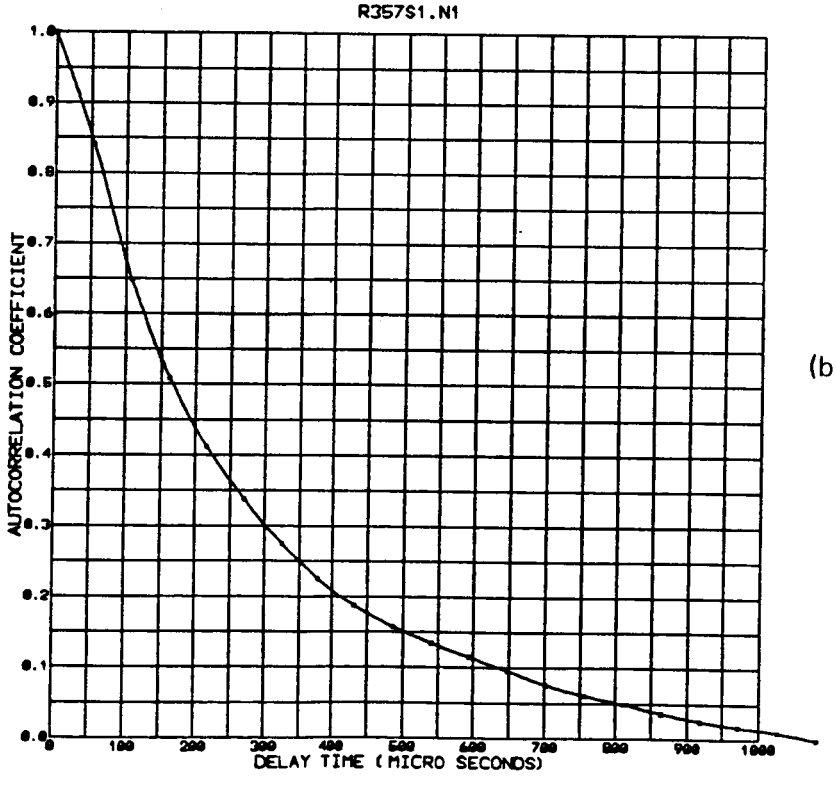

(b)

Figure 1. Examples of typical autocorrelation coefficient measurement

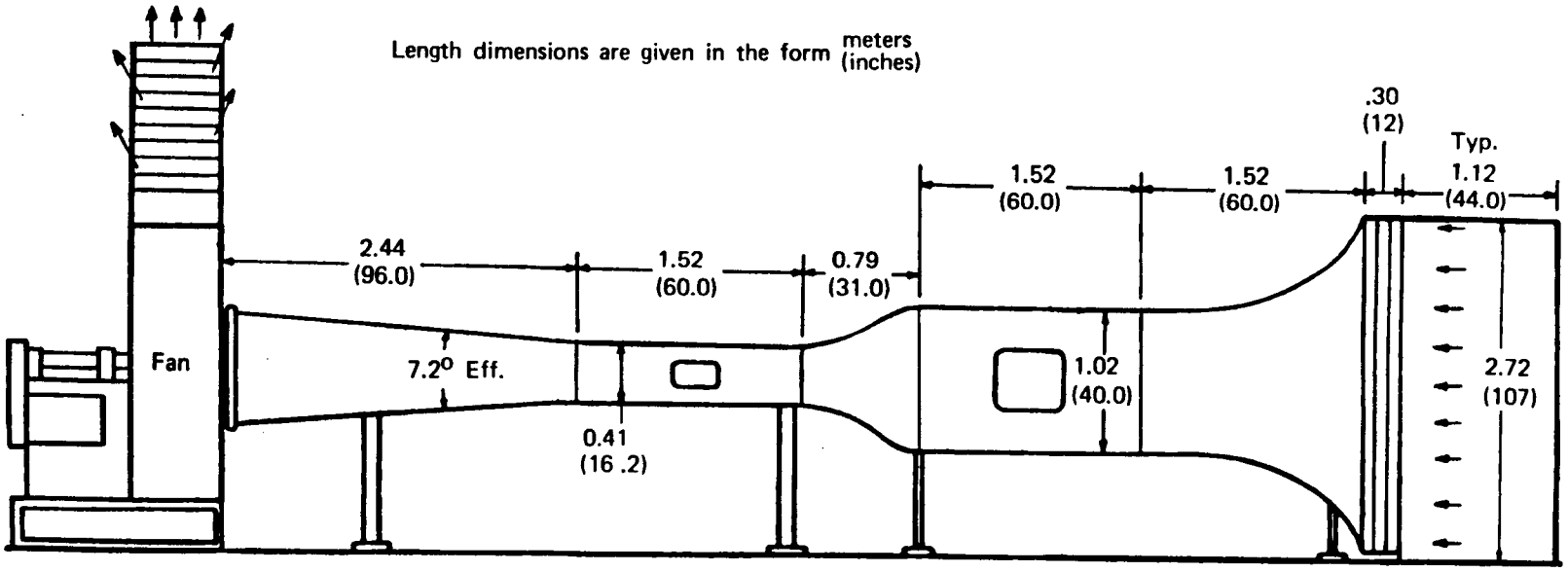

Figure 2. Elevation view of Vanderbilt University Engineering School subsonic wind tunnel

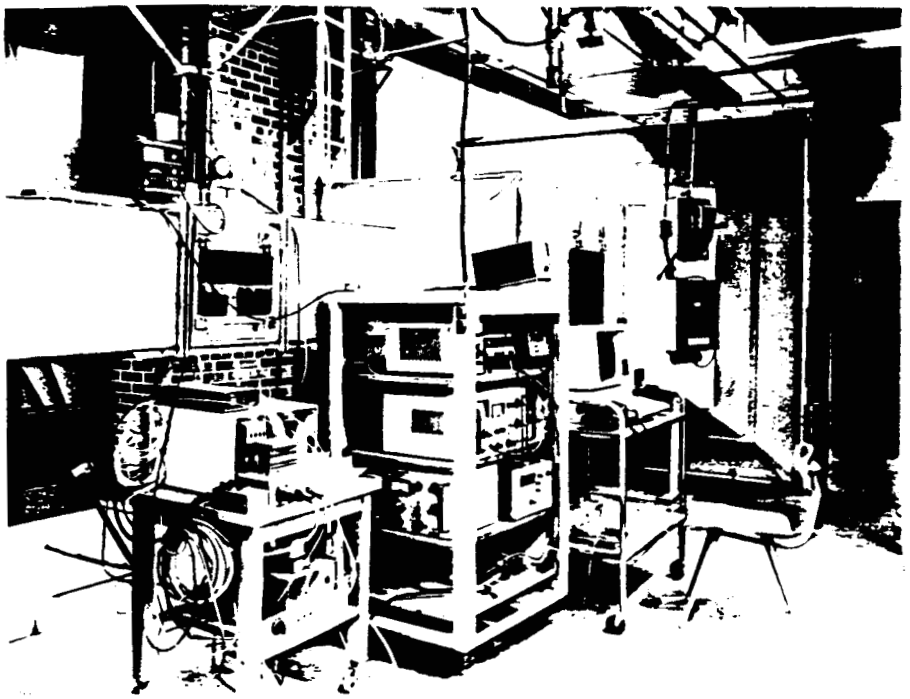

Figure 3. Photograph of working section area of wind tunnel

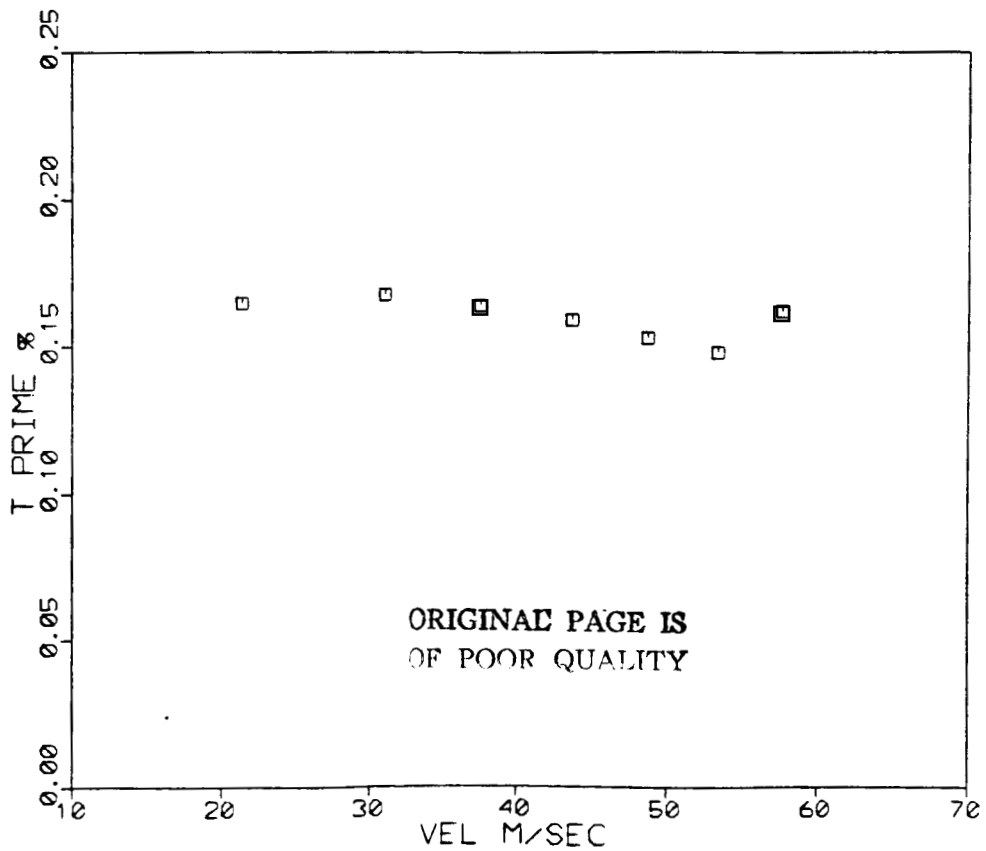

Figure 4. Relative turbulence intensity as a function of tunnel free-stream velocity

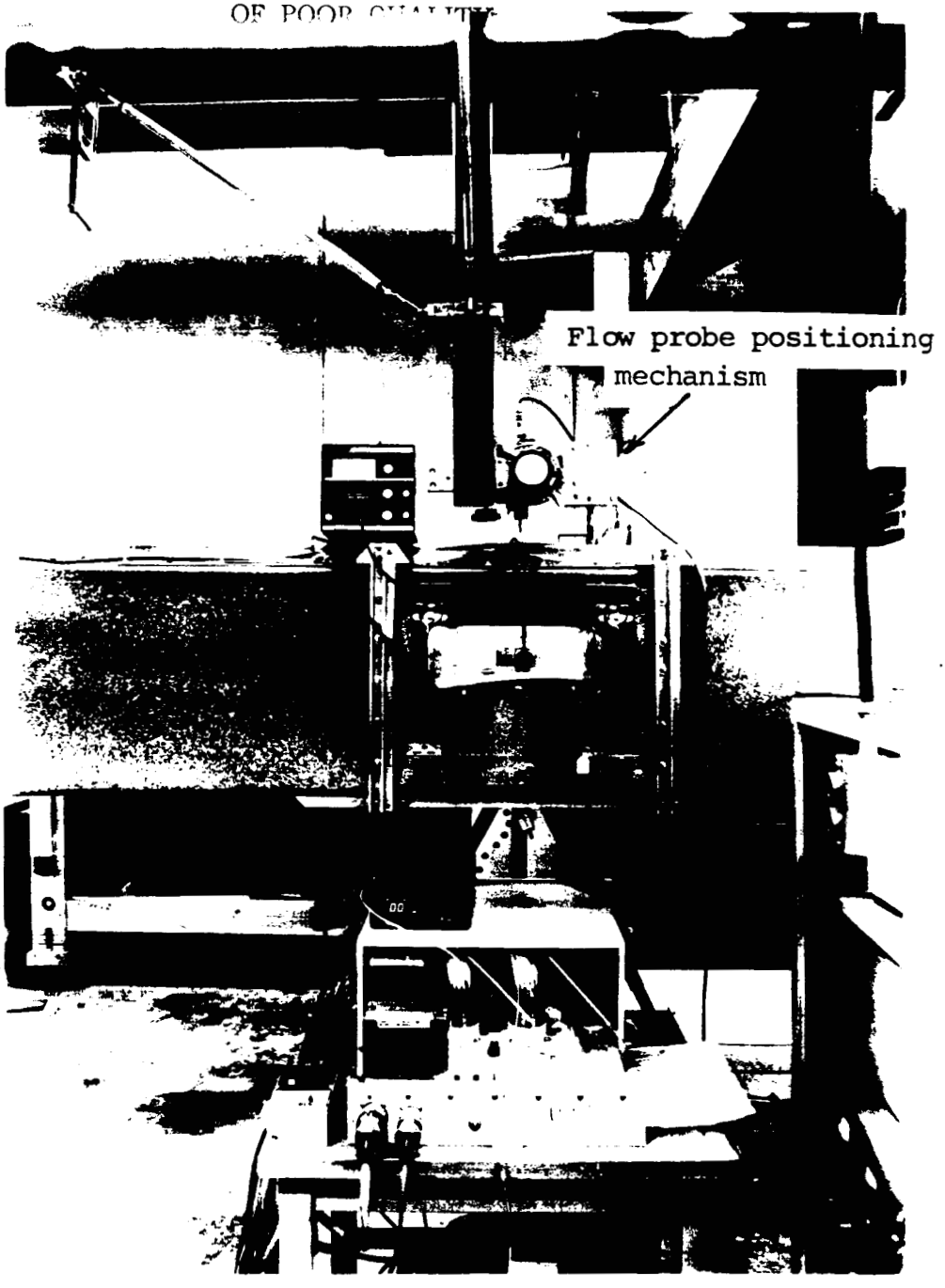

Figure 5. Flow probe support structure

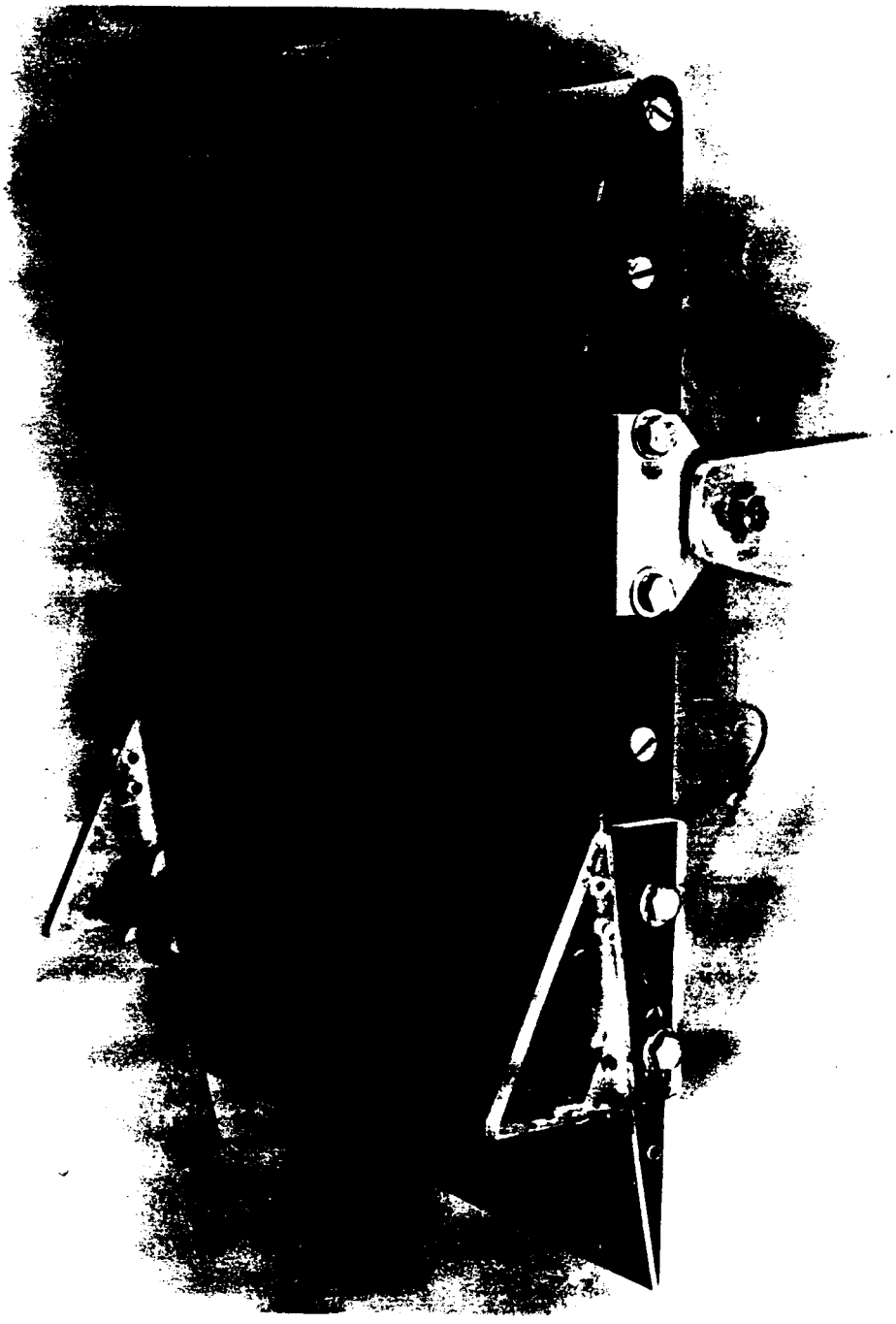

Figure 6. Airfoil and mounting system

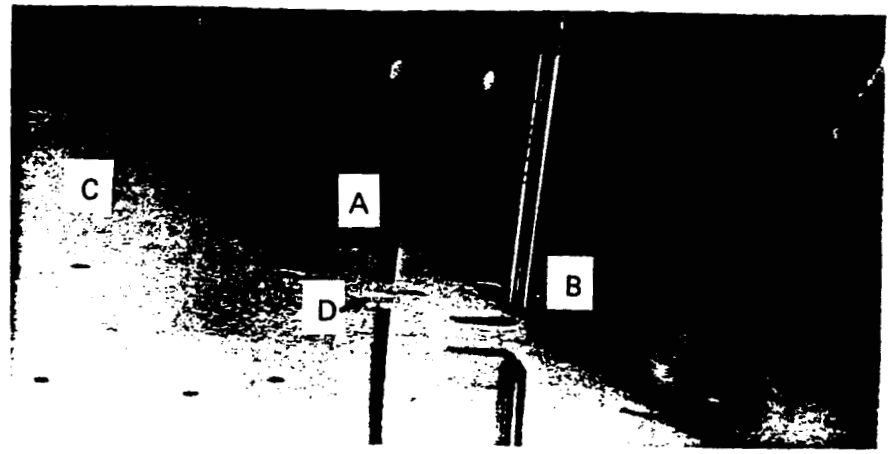

Figure 7. Fiber-optic surface-sensing device and a hot-wire probe

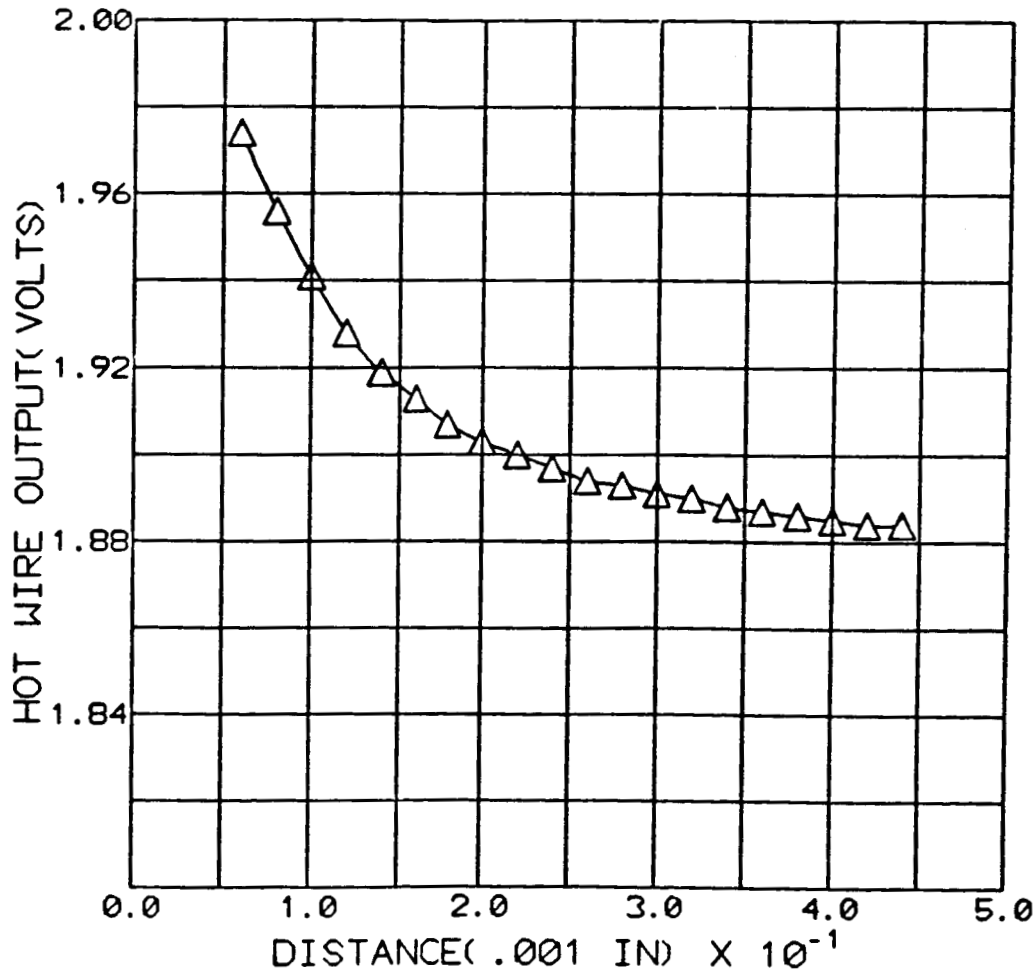

Figure 8. Variation of hot-wire signal with distance from surface of model at $U_\infty = 0$

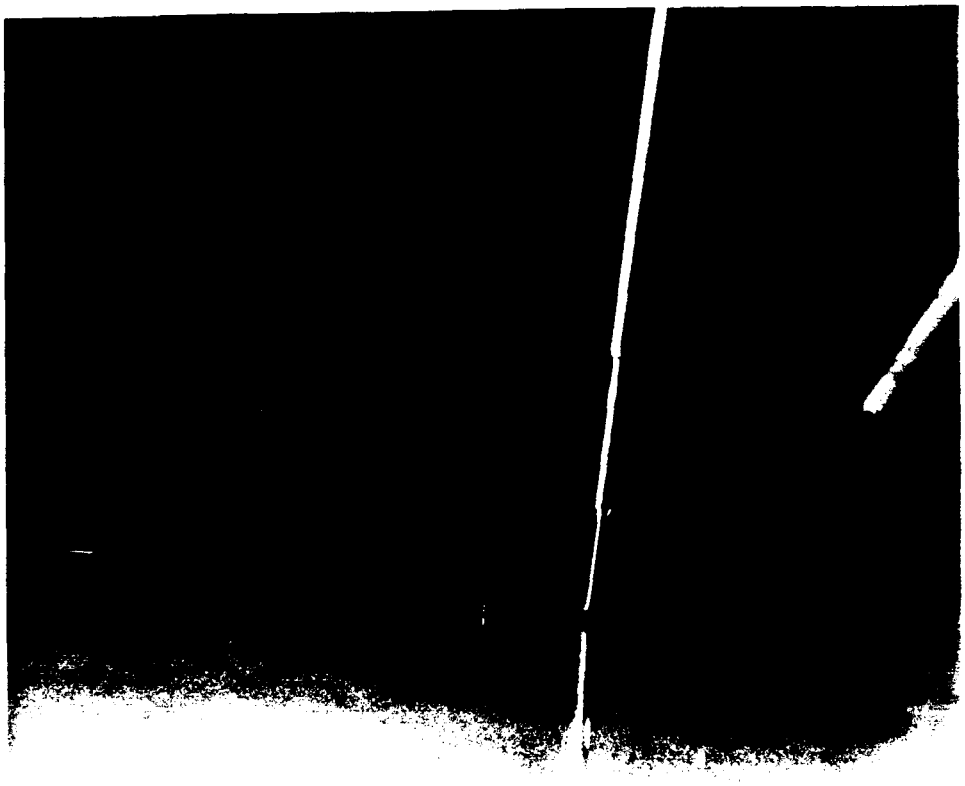

Figure 9. Photograph of Preston tube

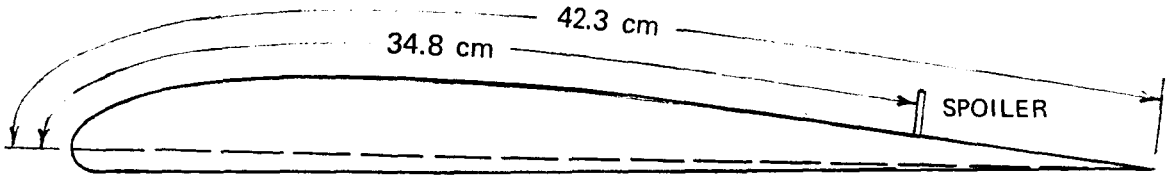

Figure 10. Sketch of airfoil cross section with spoiler

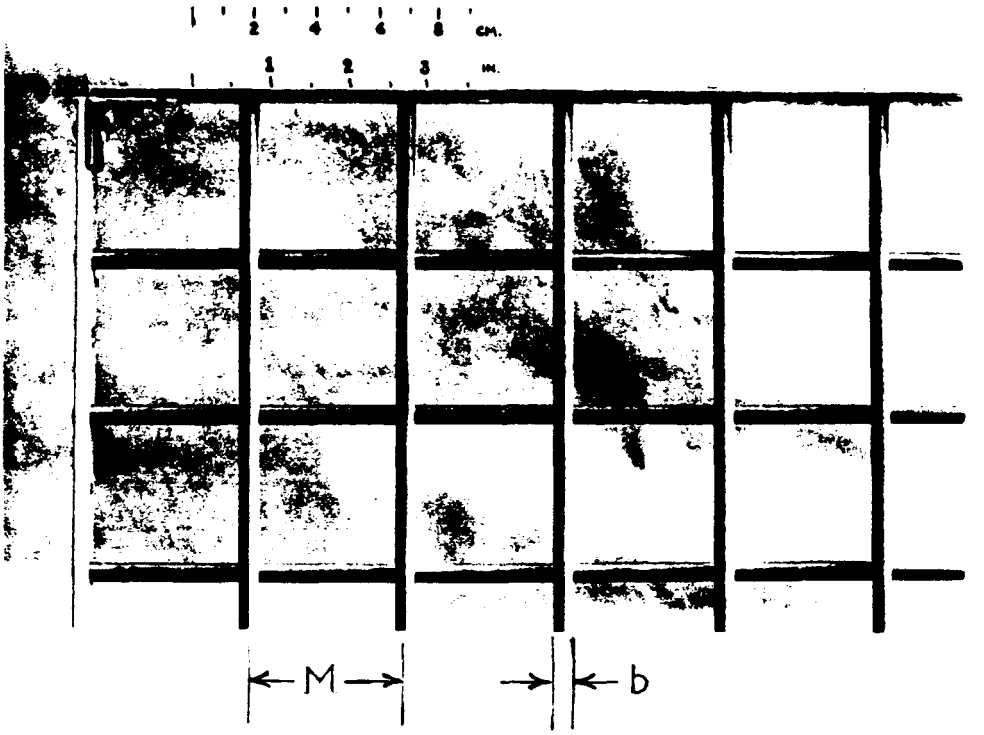

GRID NO.	M CM	b CM	GRID ELEMENT CROSS SECTION
1	10.16	1.24	RECTANGULAR*
2	5.08	0.32	ROUND
3	5.08	1.24	RECTANGULAR*
4	2.54	0.64	ROUND
5	5.08	0.64	ROUND

*1.87 CM IN STREAMWISE DIRECTION

Figure 11. Dimensions of turbulence-producing grids

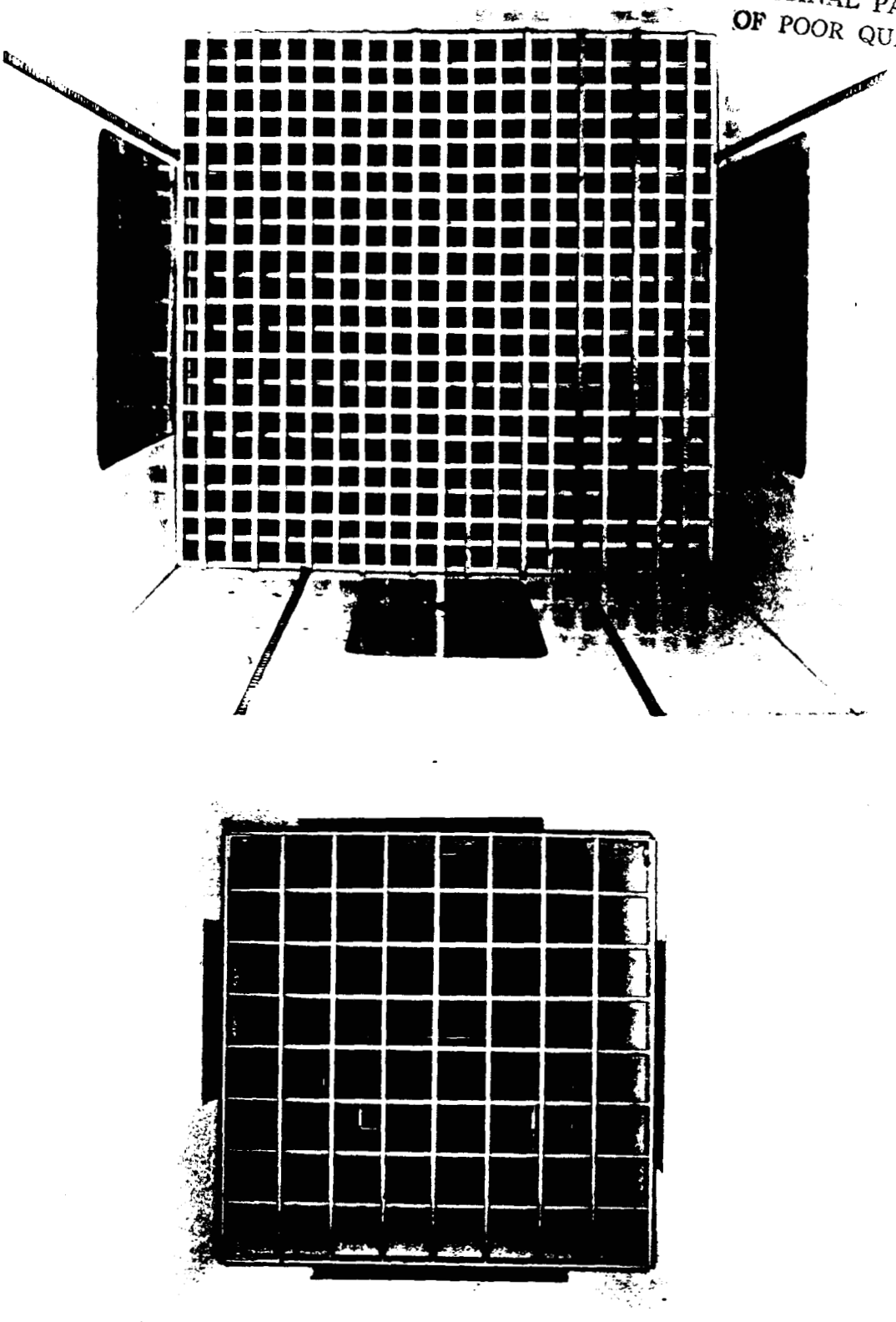

Figure 12. Typical grid installations

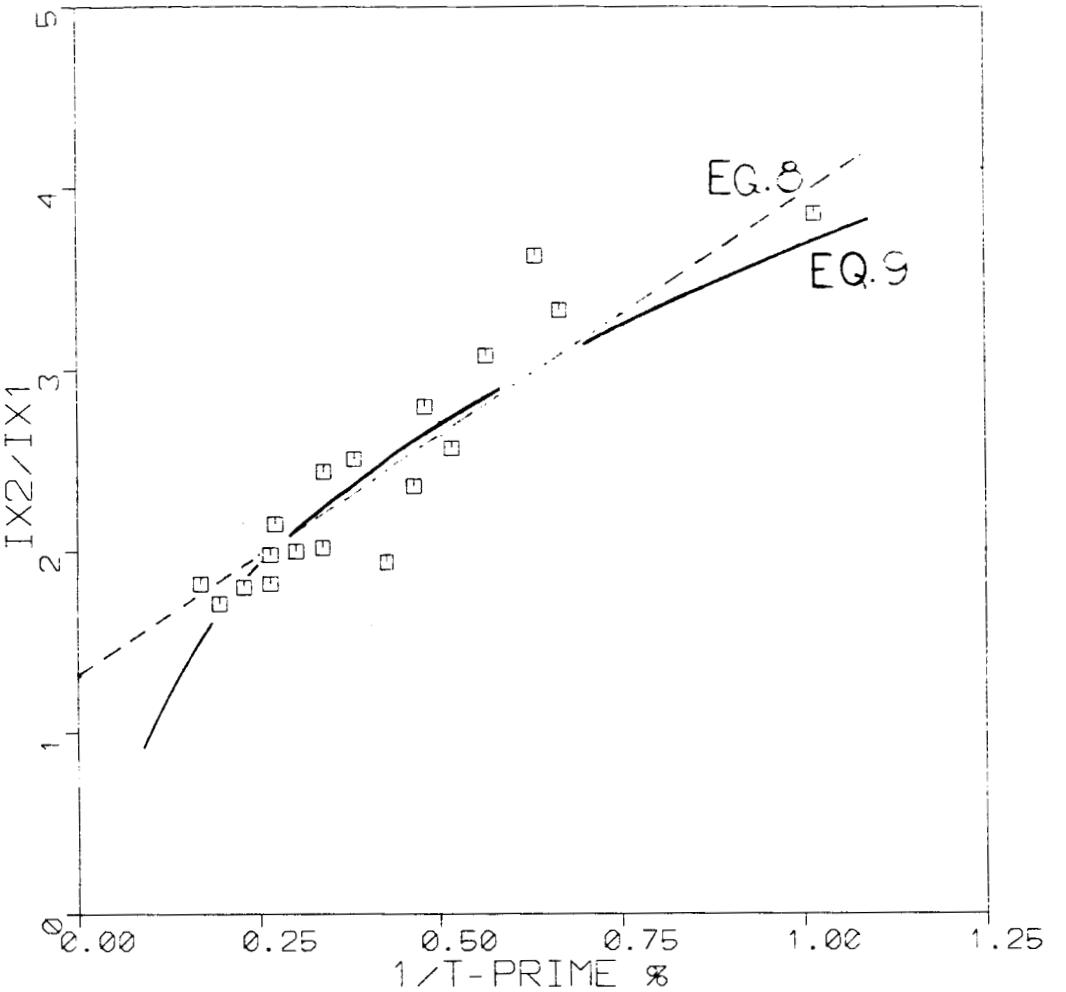

Figure 13. Effect of wind tunnel contraction on integral scales

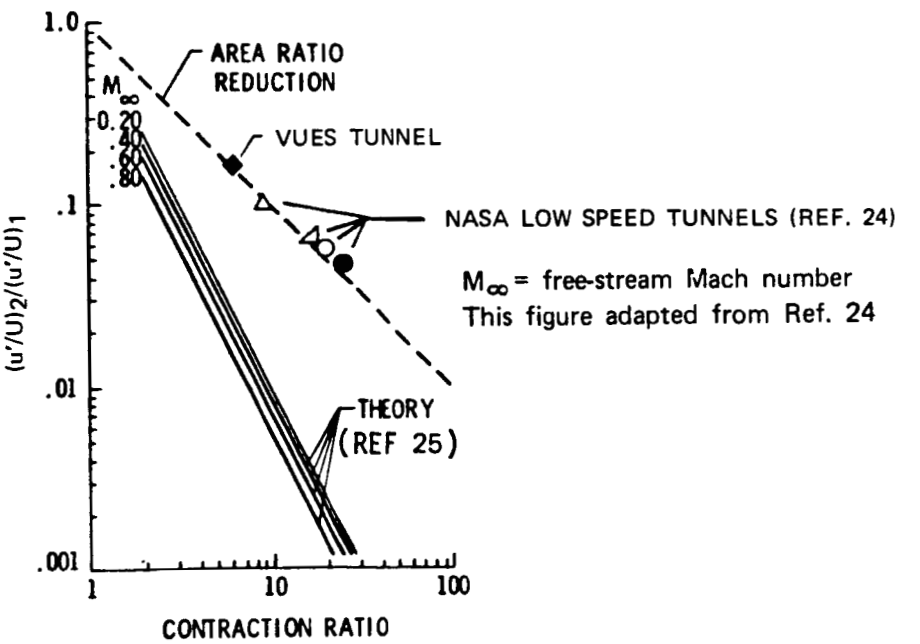

Figure 14. Effect of wind tunnel contraction on relative turbulence intensity

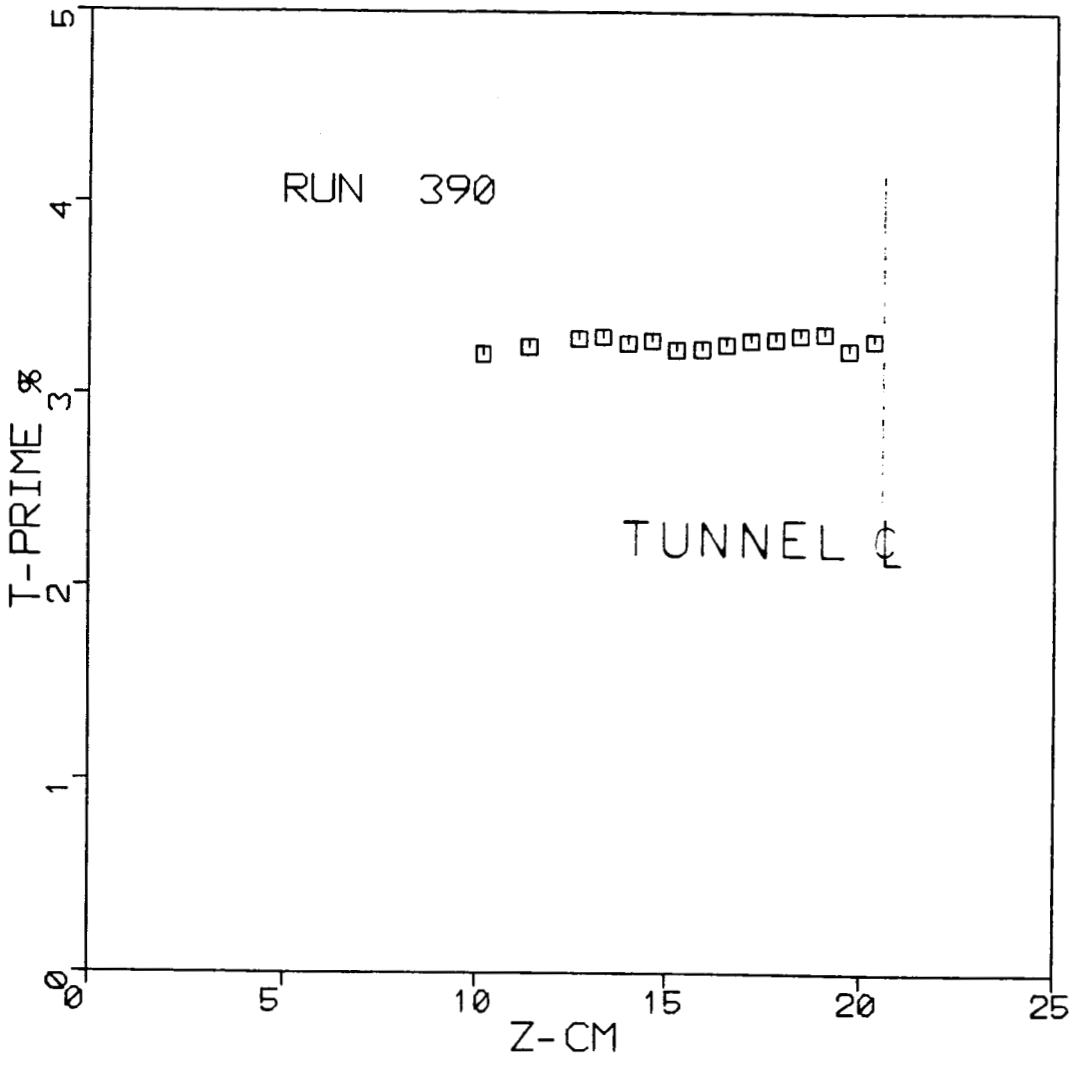

Figure 15. Cross-stream distribution of T'_∞ with minimum X/M grid #5

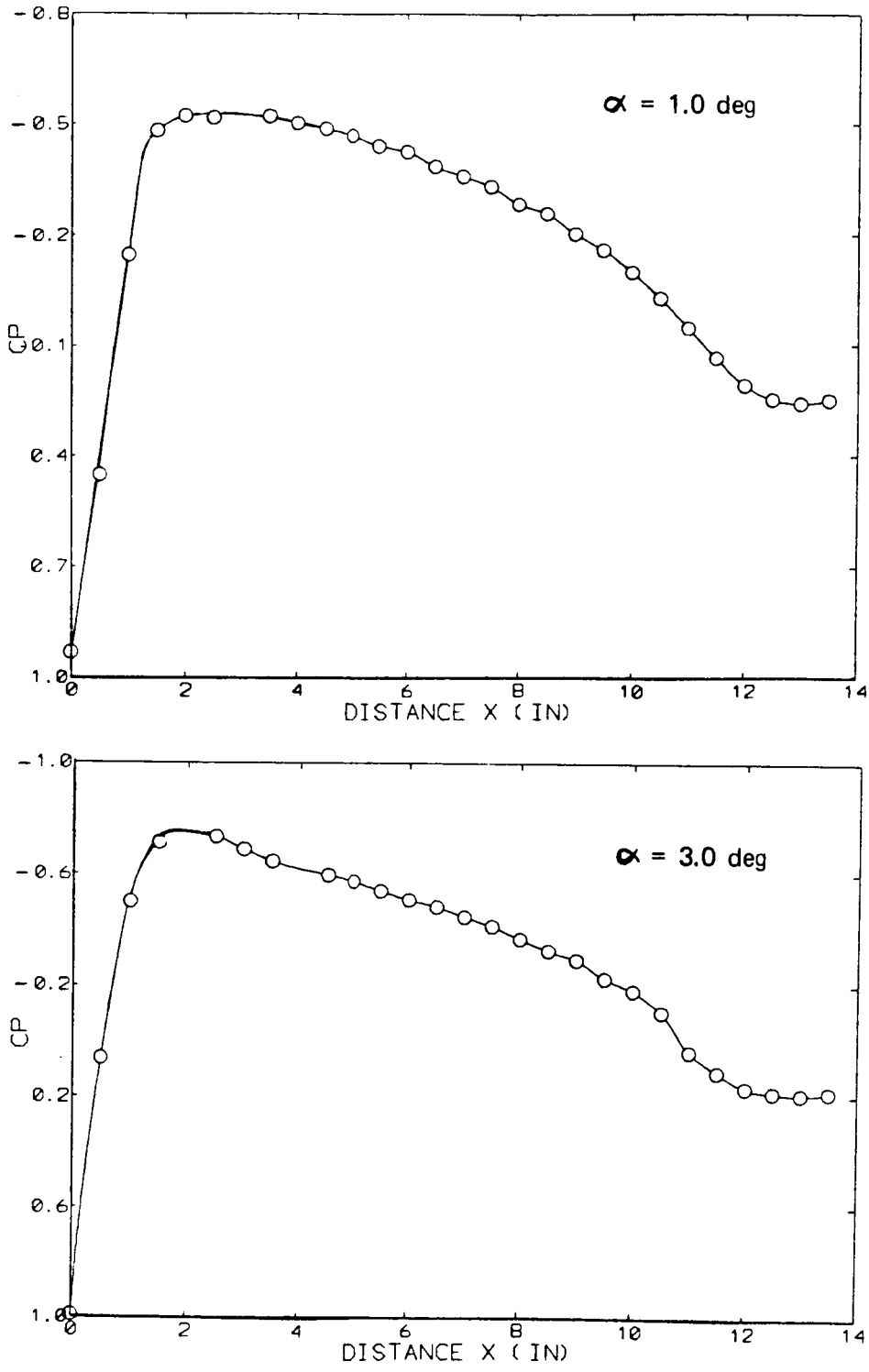

Figure 16. Pressure distributions on the airfoil

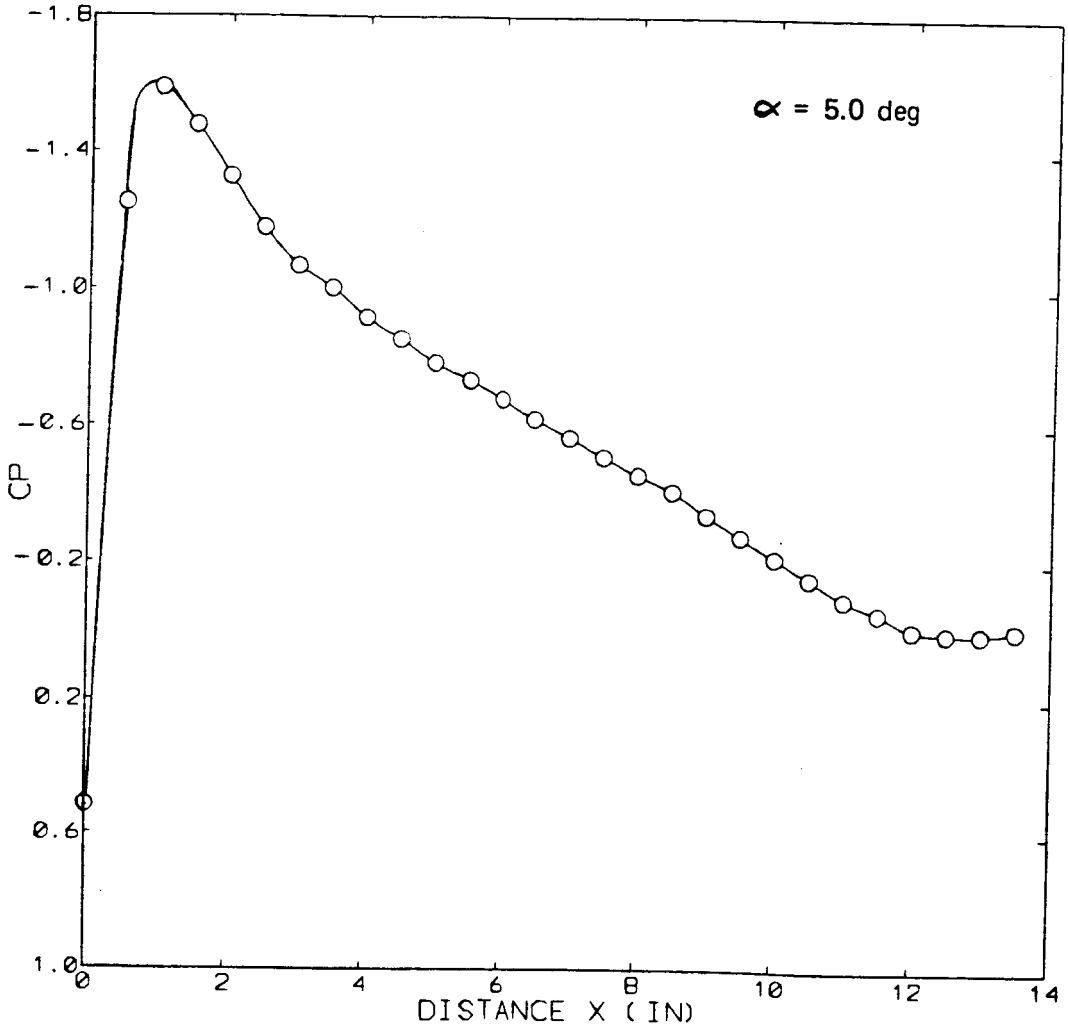

(d)

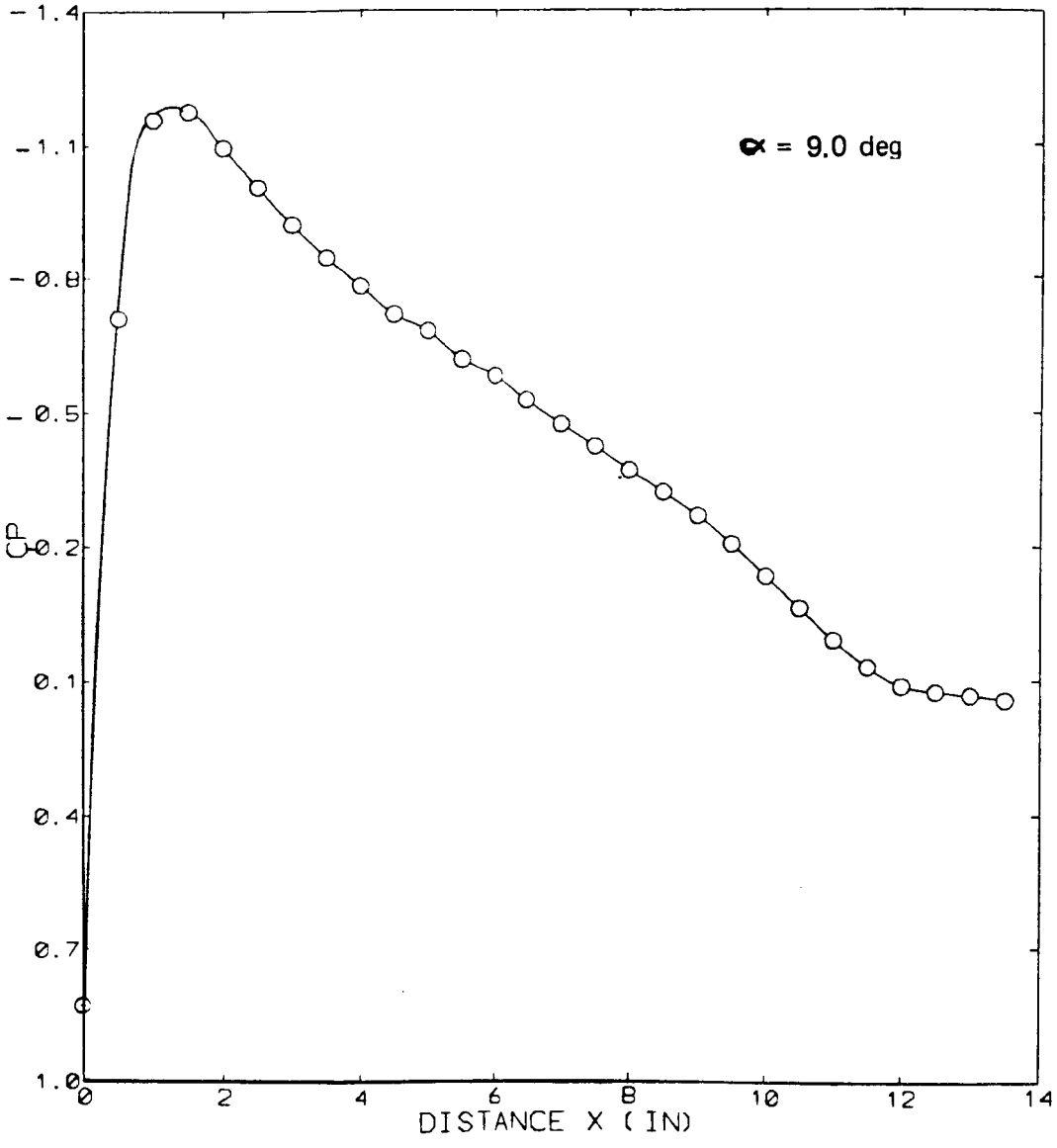

(c)

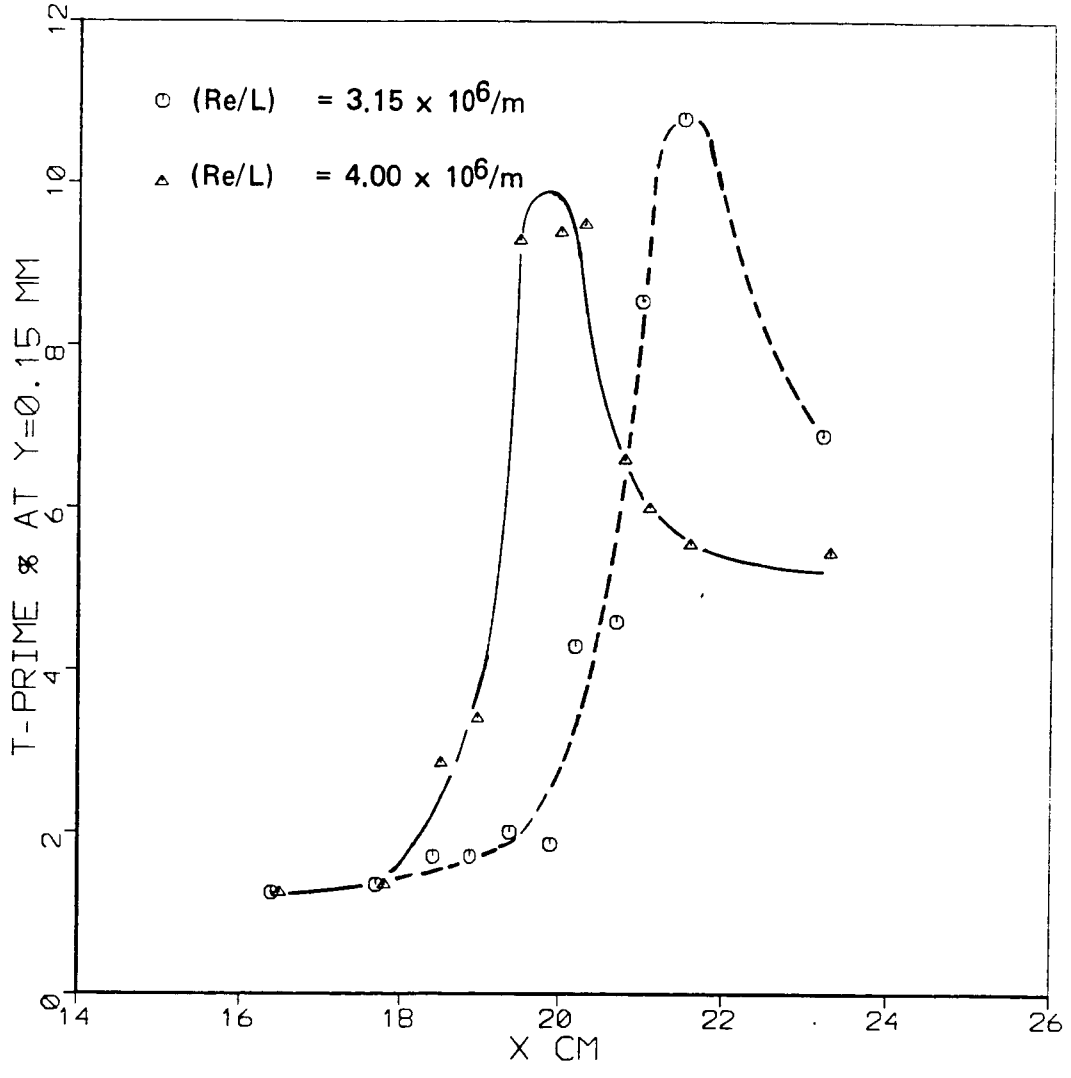

Figure 17. Transition locations on the airfoil with no boundary layer trips and no grids

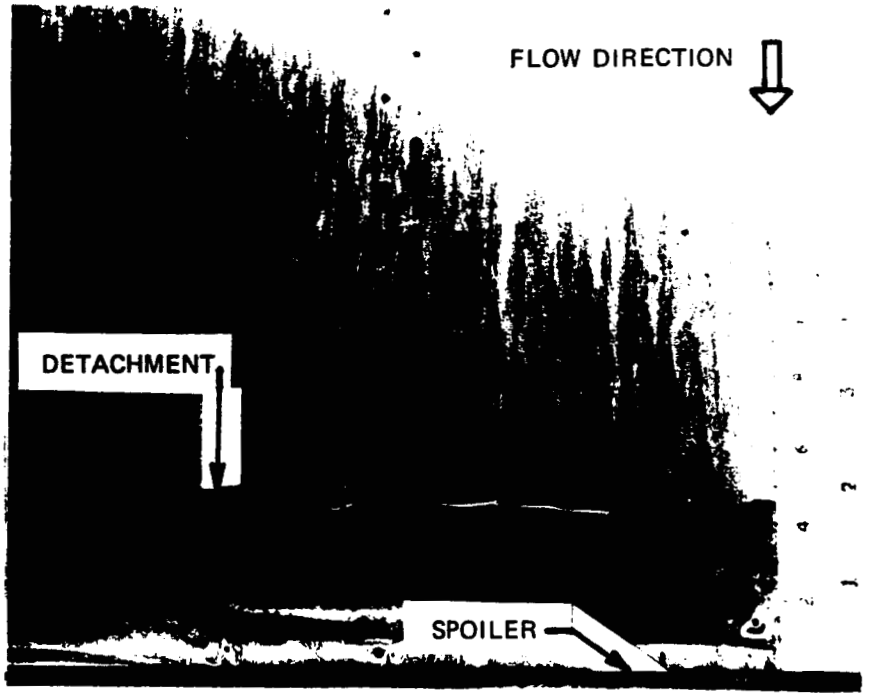

Figure 18. Liquid-film data on the separation zone: overhead views

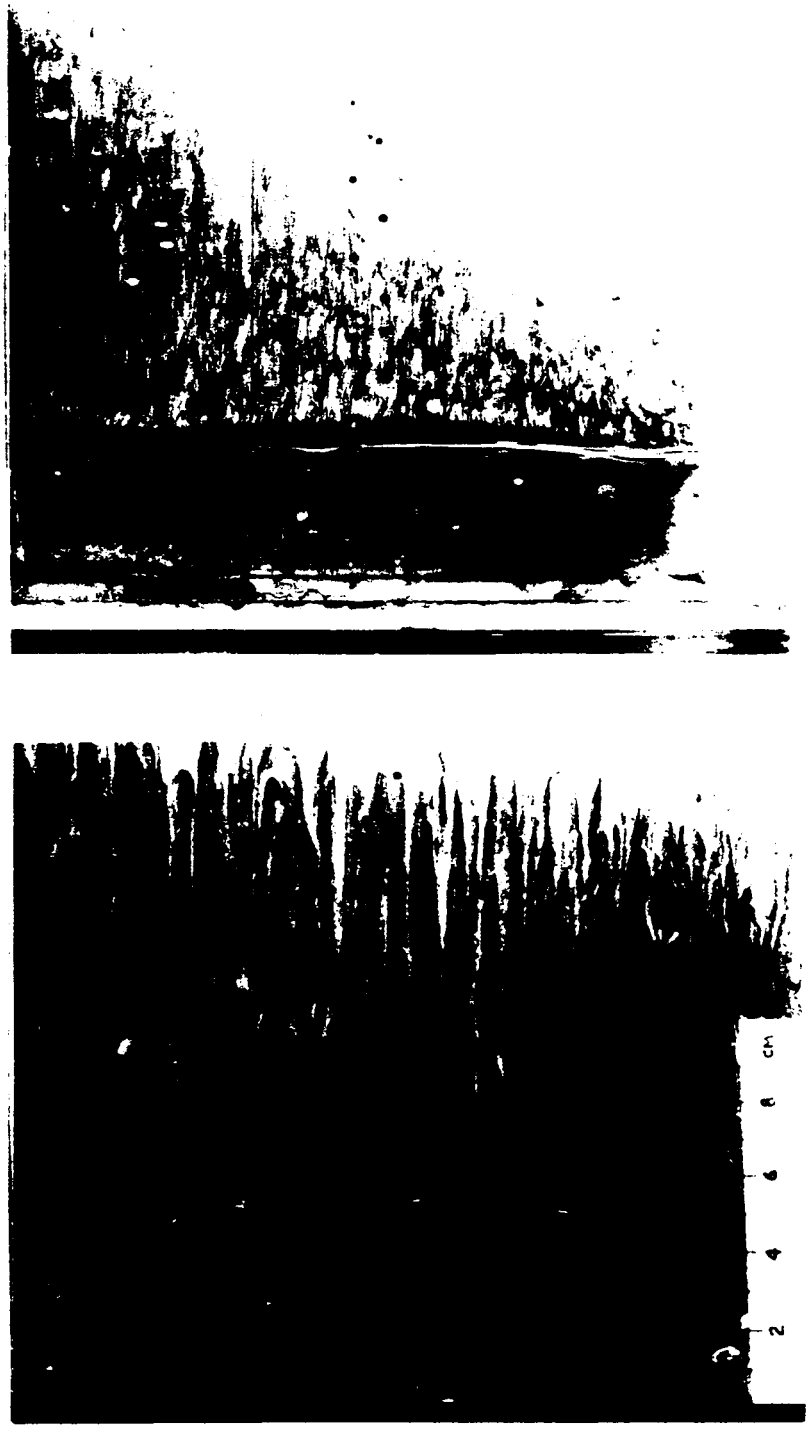

Figure 18 cont'd.

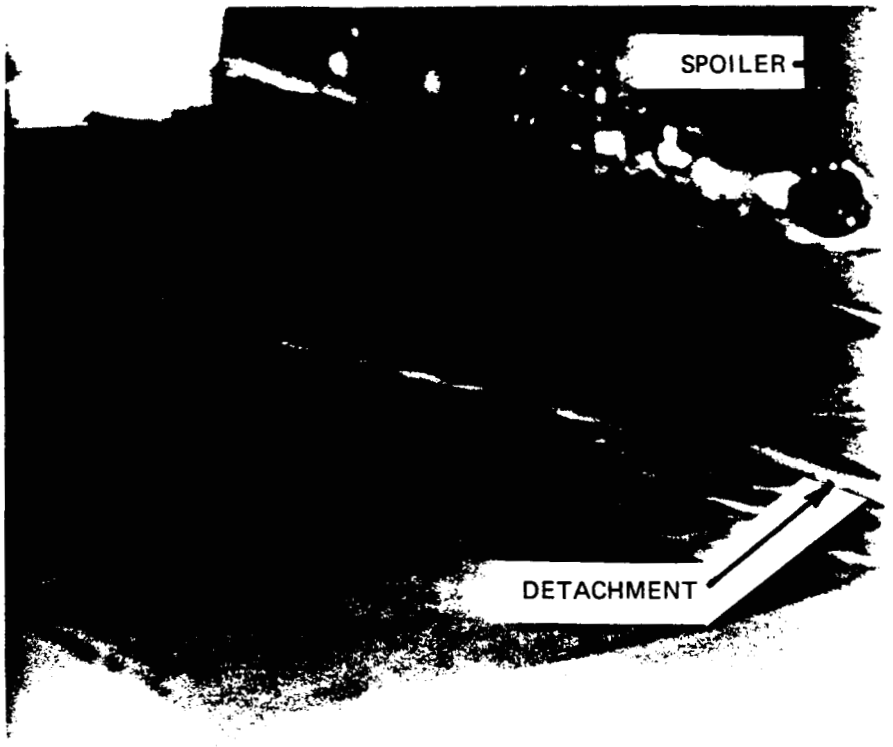

Figure 19. Liquid-film result viewed at oblique angle

(a)

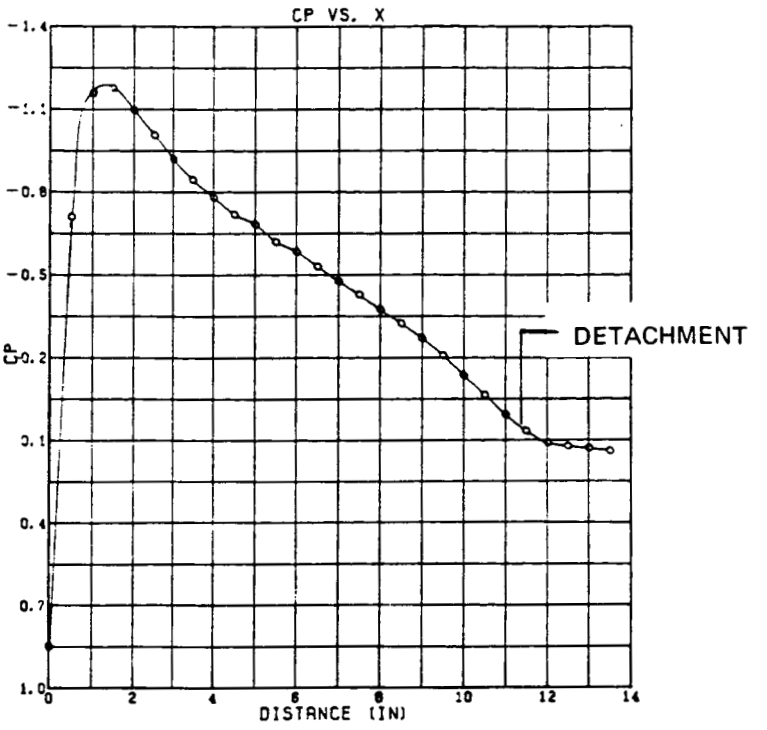

(b)

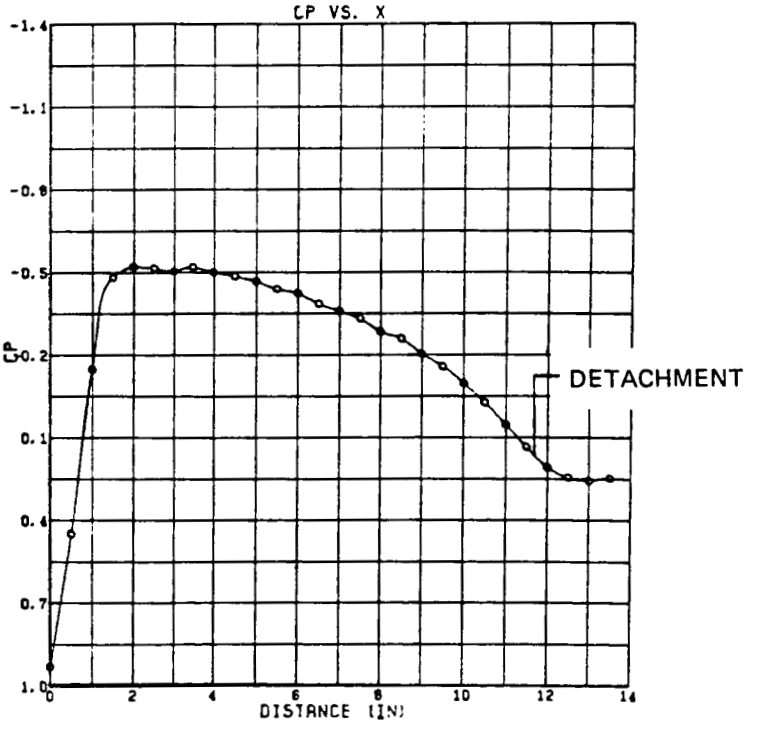

Figure 20. Pressure distributions and corresponding liquid-film evidence of detachment

	I_{x_∞} cm	T'_∞ %
○	0.74	2.85
×	"	0.38
△	"	0.31

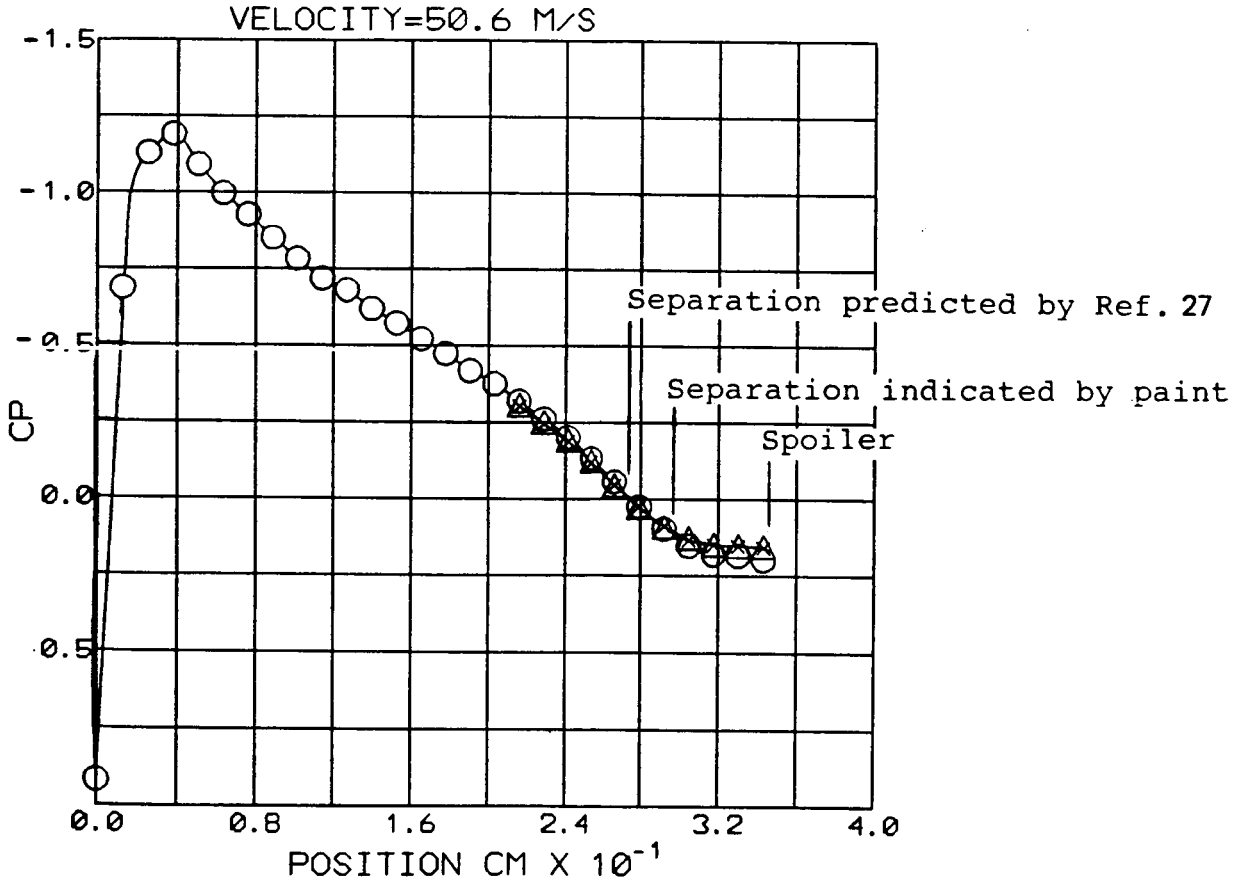

Figure 21. Pressure coefficient and liquid-film results for varying turbulence intensity

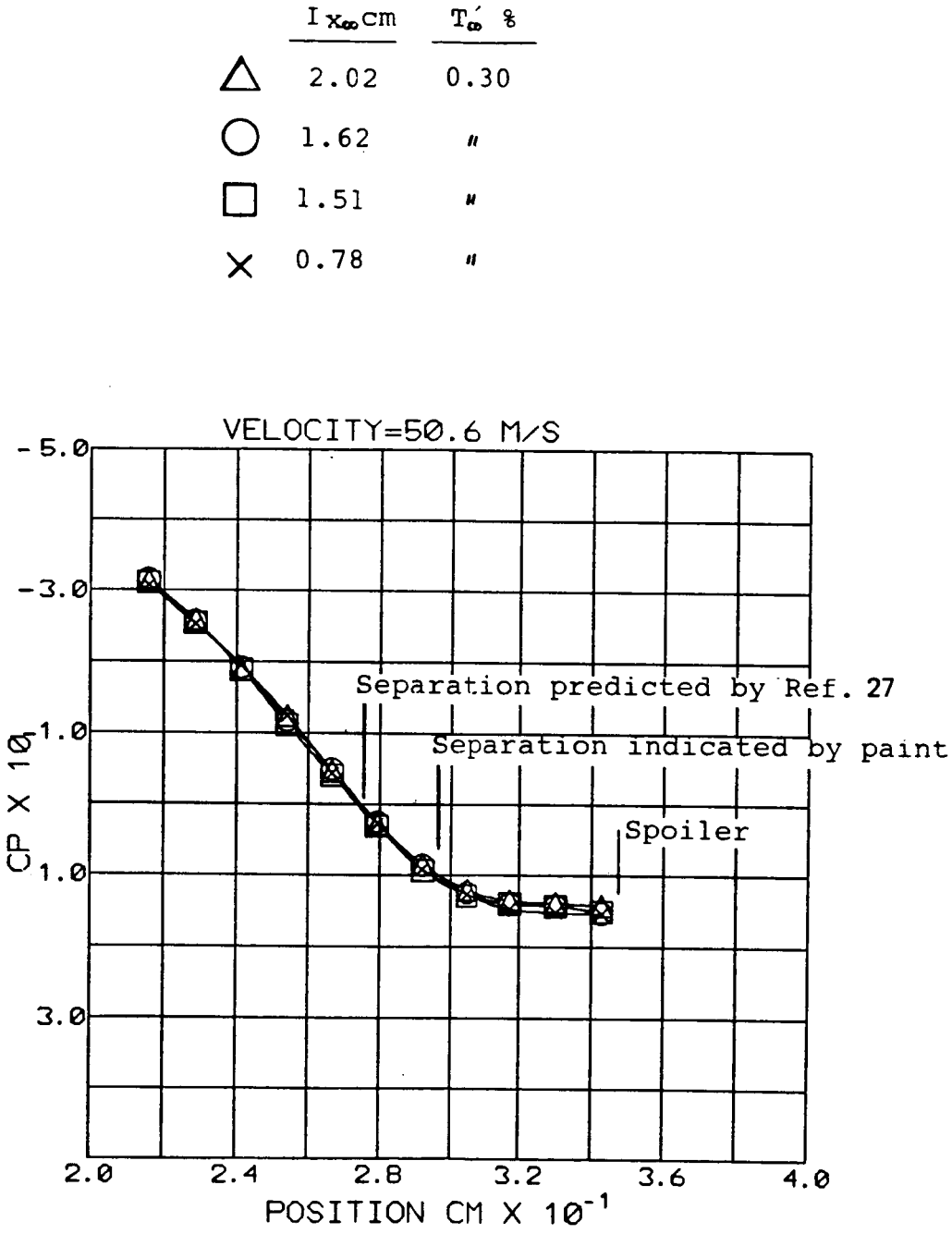

Figure 22. Pressure coefficient and liquid-film results for varying integral scale

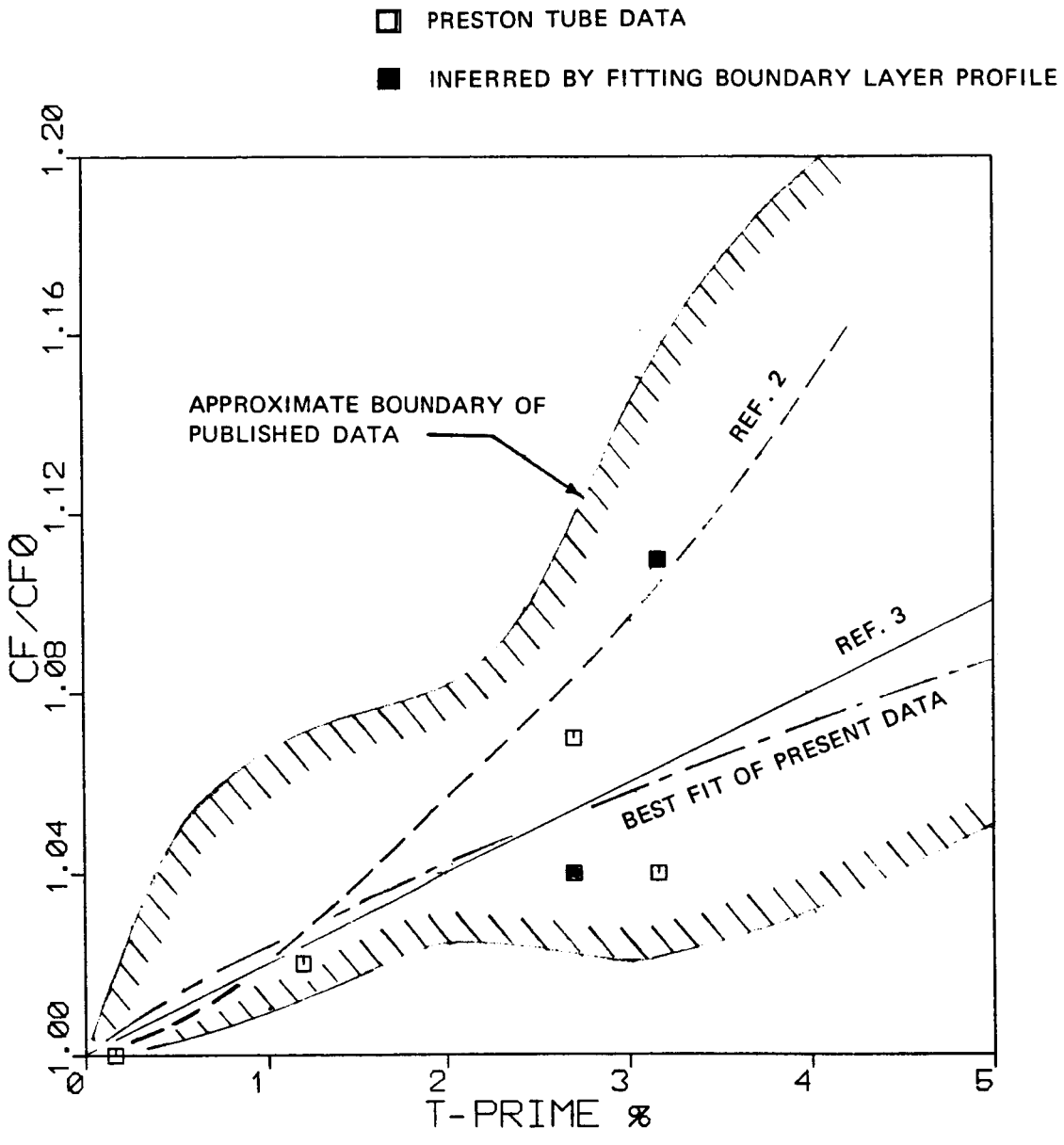

Figure 23. The effect of turbulence intensity upon skin friction

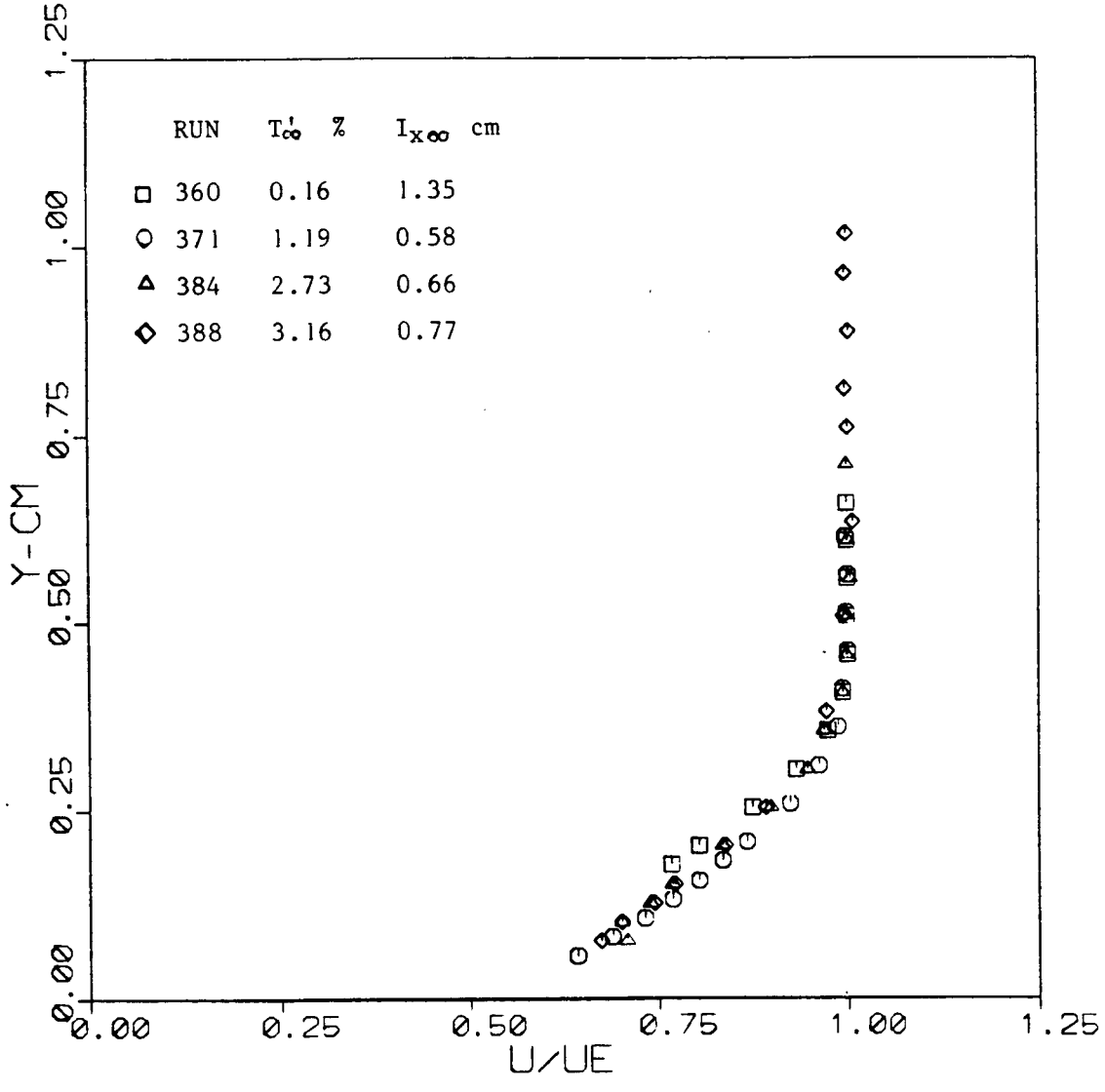

Figure 24. Boundary layer velocity profiles for varying free-stream turbulence: x = 22.1 cm

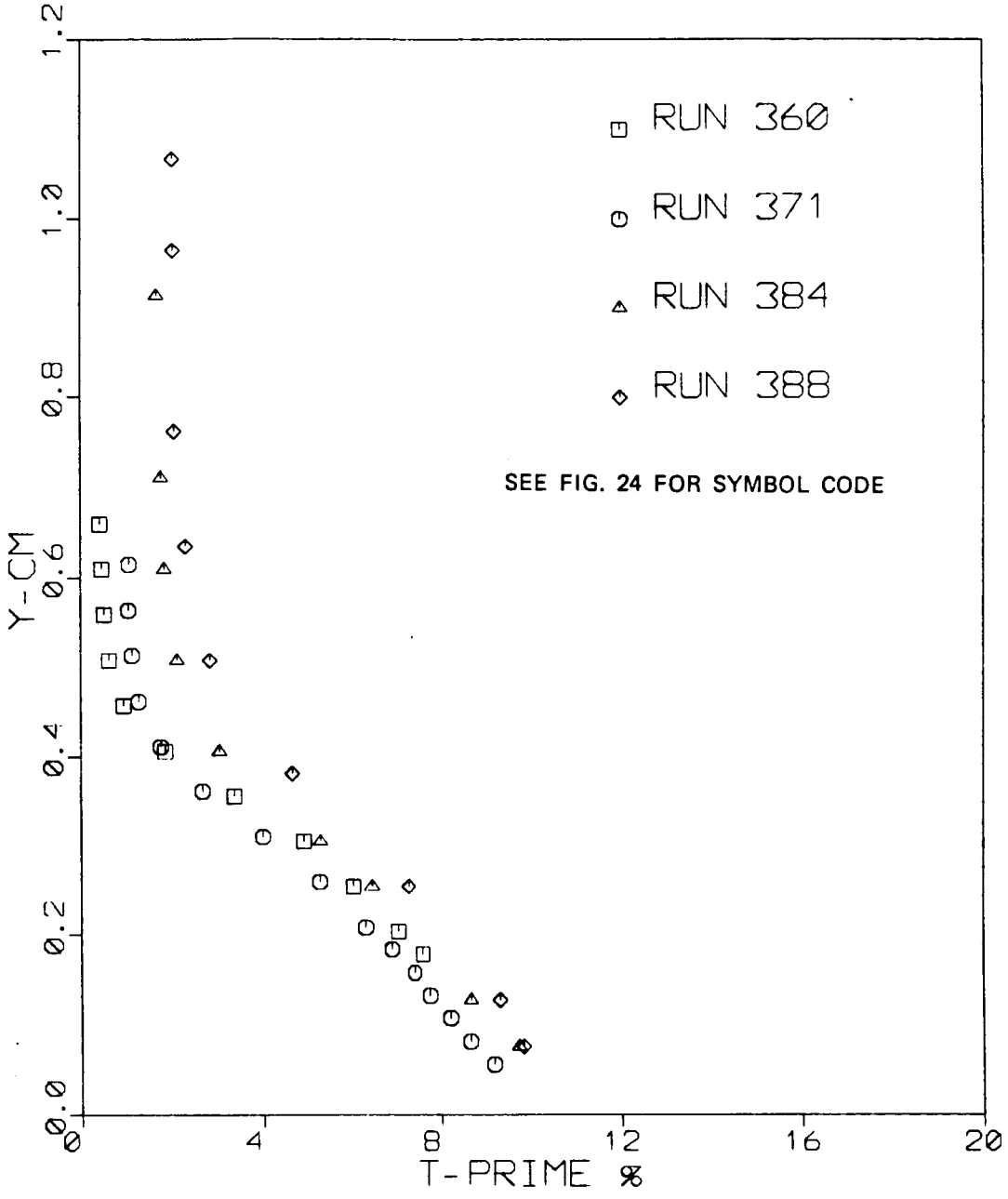

Figure 25. Boundary layer turbulence intensity profiles for varying free-stream turbulence: x = 22.1 cm

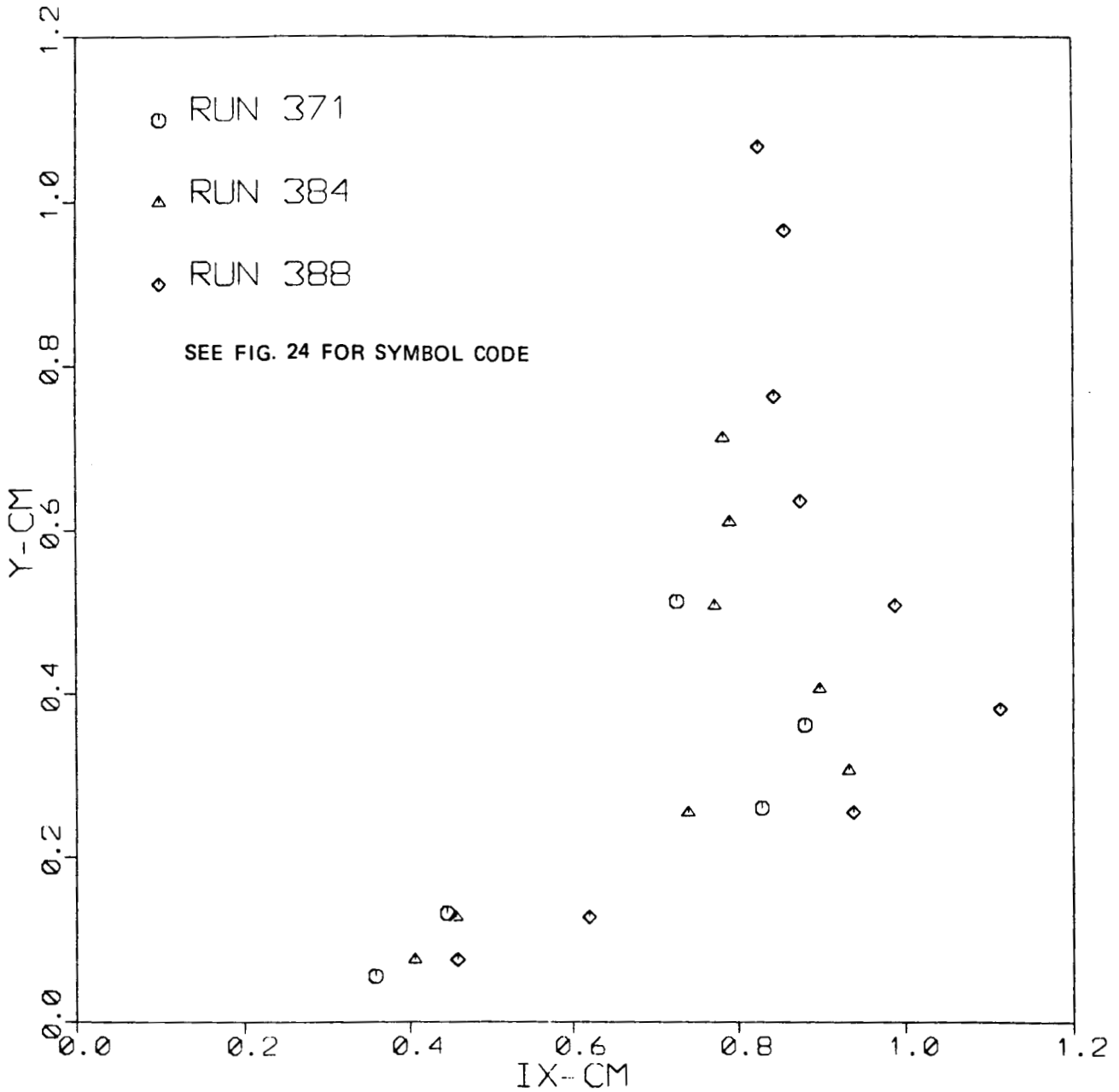

Figure 26. Boundary layer integral scale profiles for varying free-stream turbulence: x = 22.1 cm

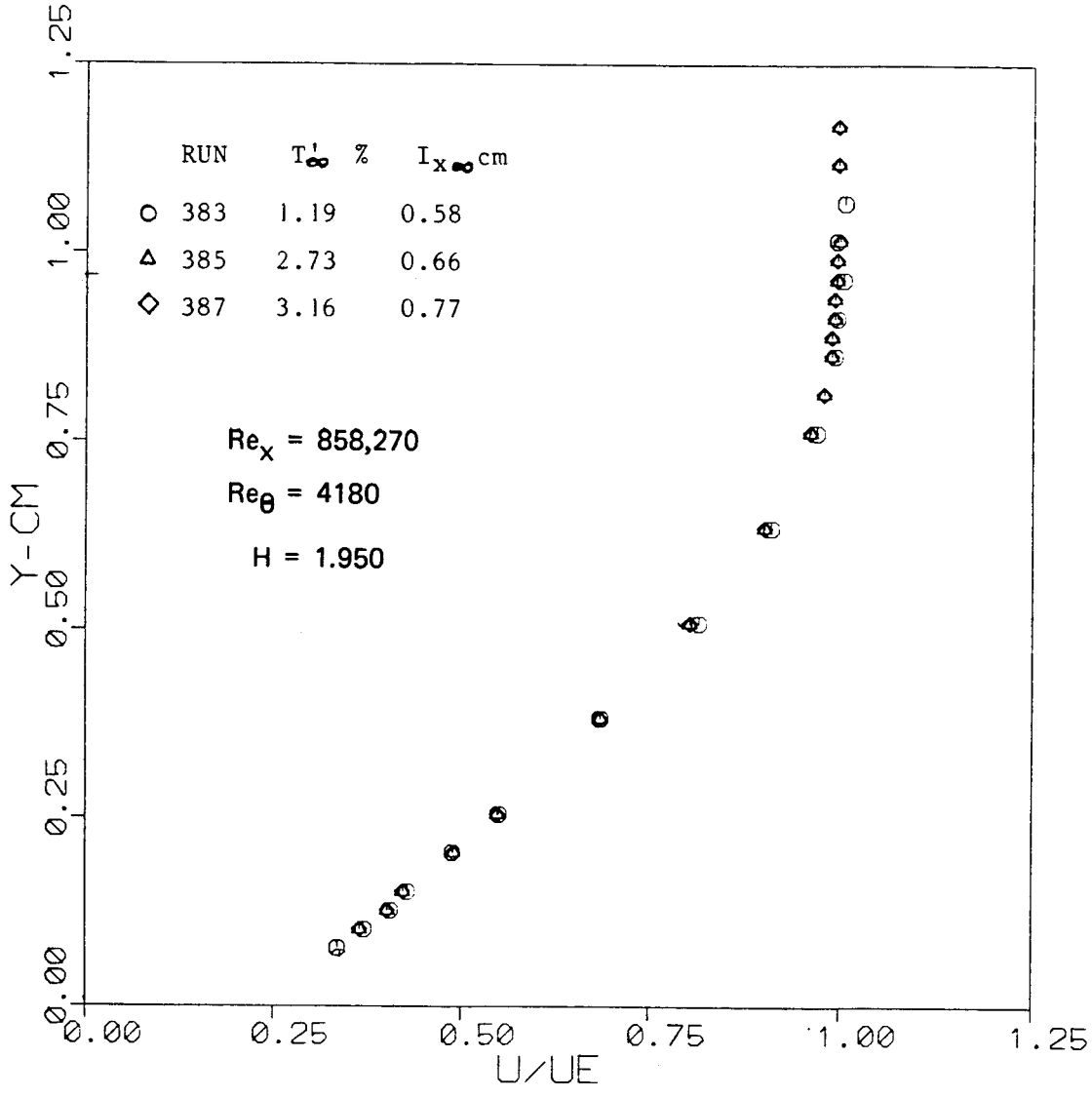

Figure 27. Boundary layer velocity profiles for varying free-stream turbulence: x = 29.7 cm

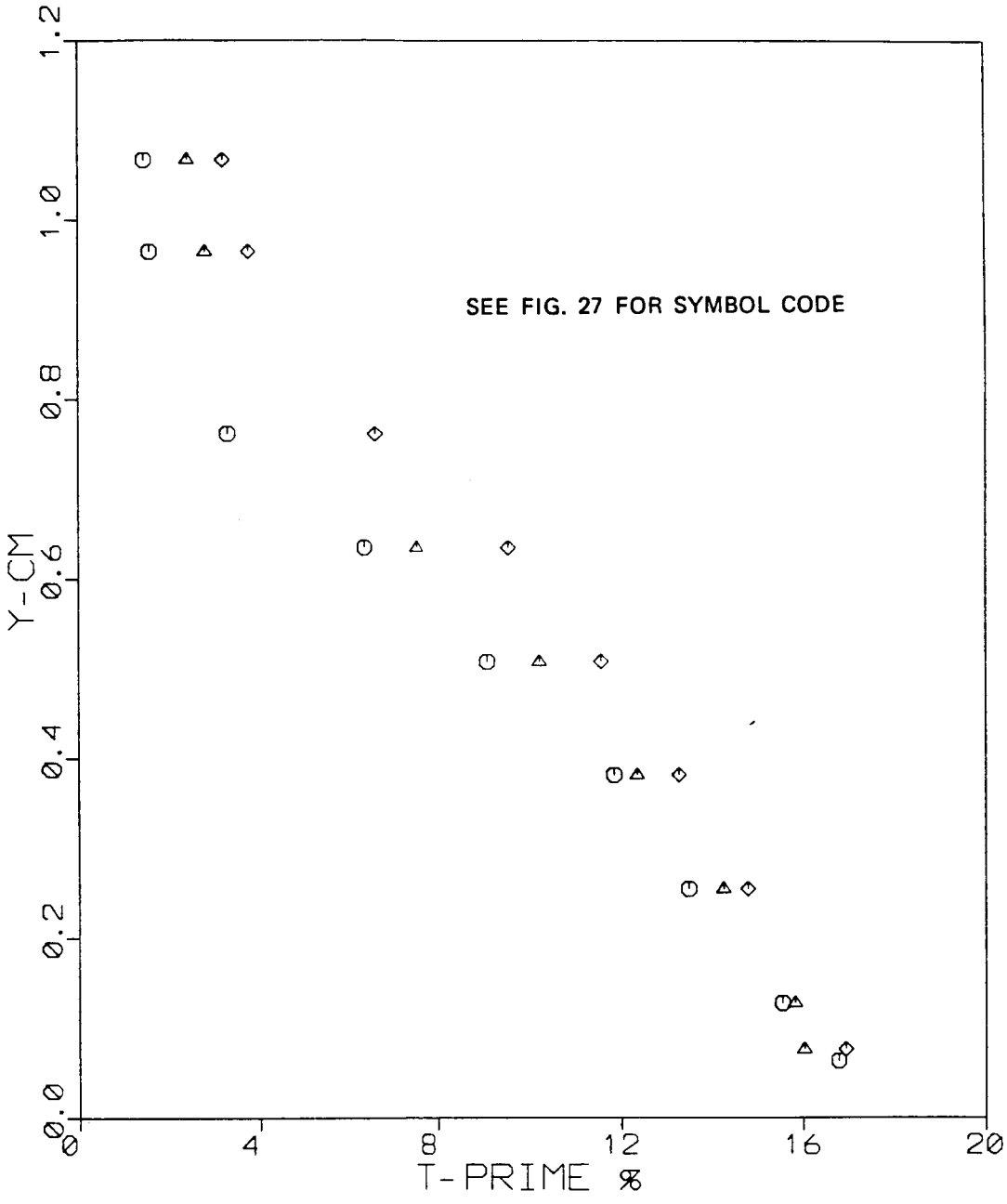

Figure 28. Boundary layer turbulence intensity profiles for varying free-stream turbulence: x = 29.7 cm

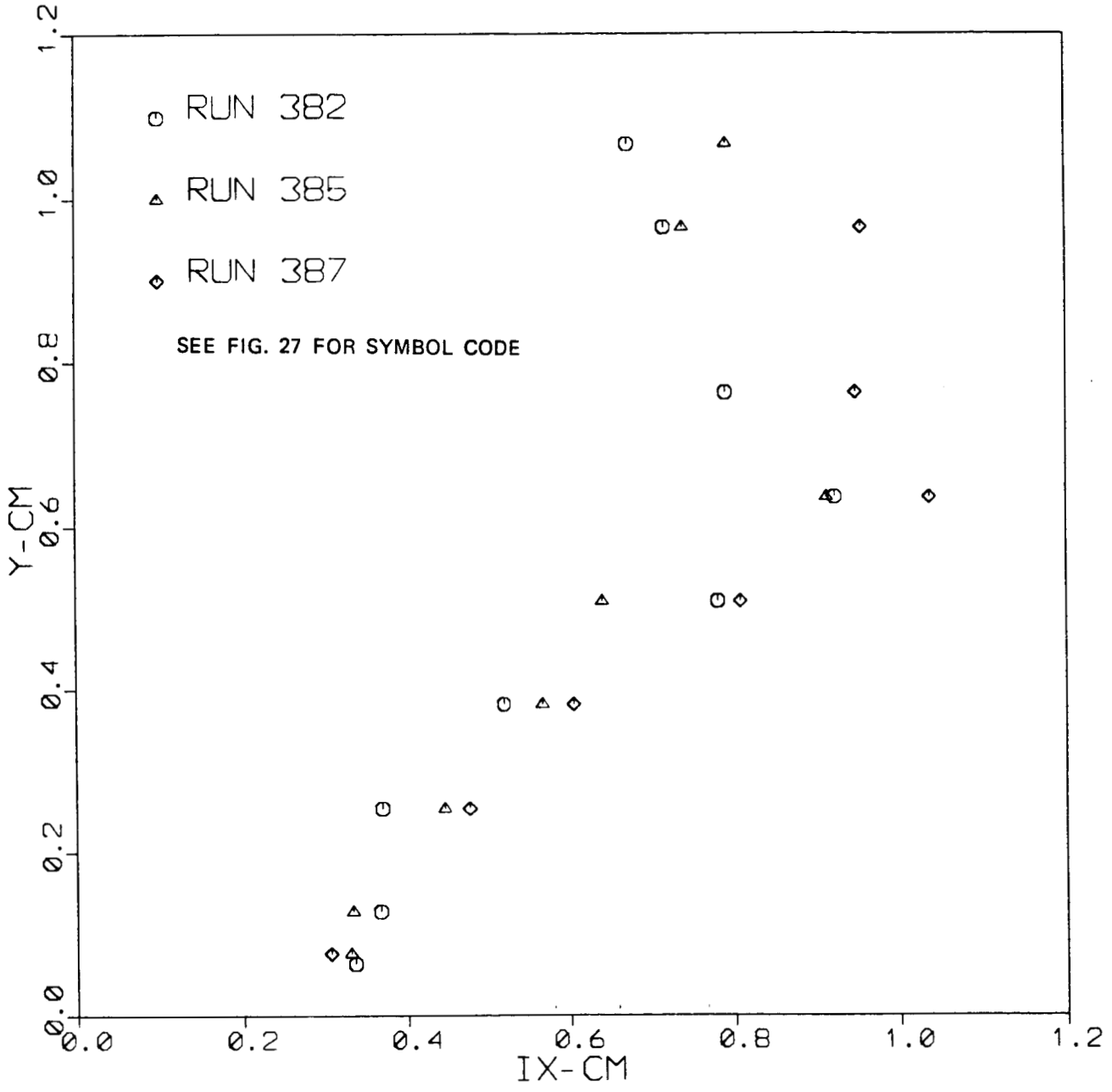

Figure 29. Boundary layer integral scale profiles for varying free-stream turbulence: x = 29.7 cm

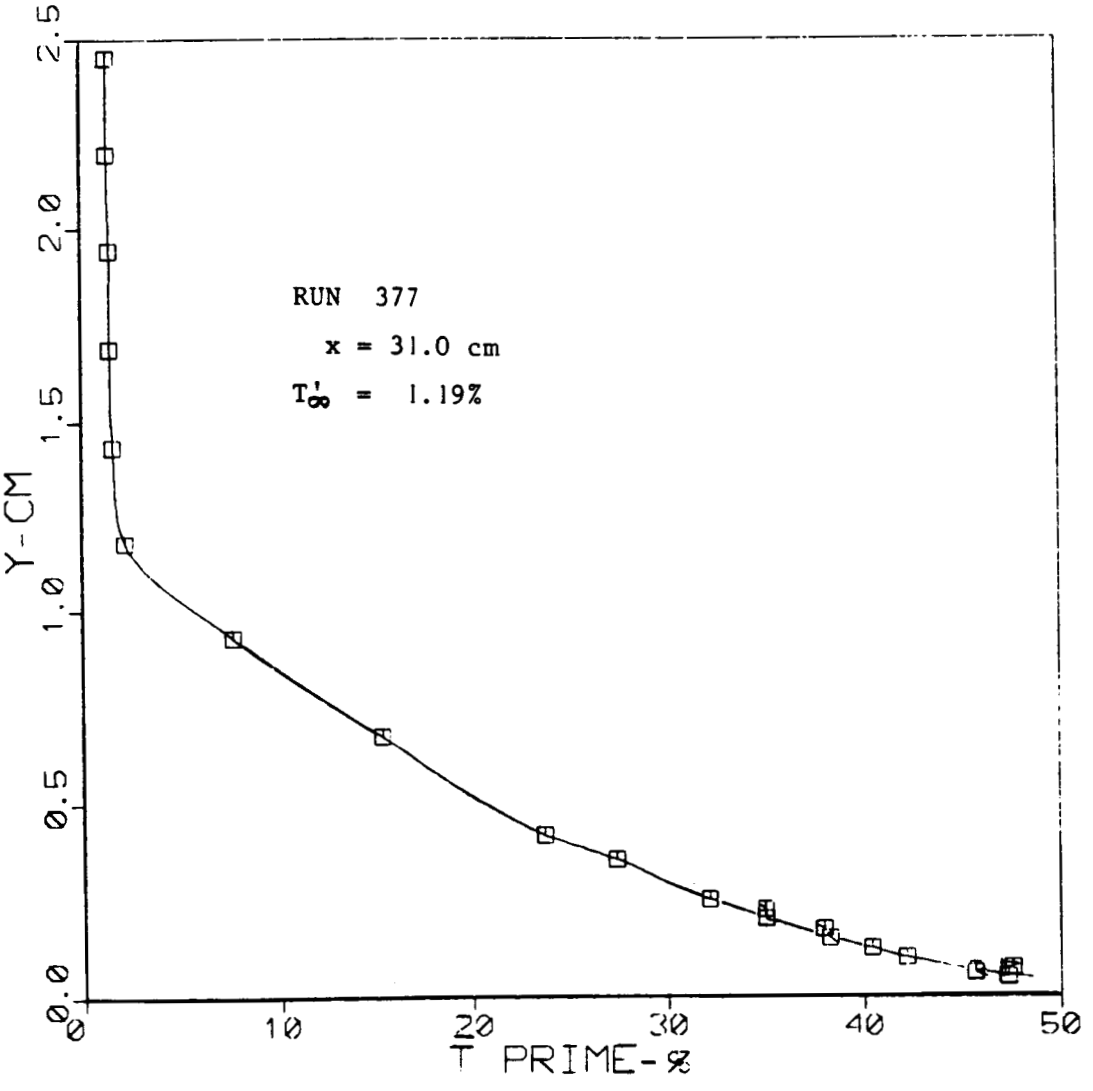

Figure 30. Example of extremely high turbulence intensity near wall in separation zone